IEEE Access
Multidisciplinary | Rapid Review | Open Access Journal

Received 9 May 2022, accepted 17 June 2022, date of publication 22 June 2022, date of current version 28 June 2022.

Digital Object Identifier 10.1109/ACCESS.2022.3185260

Overview of Metamaterials-Integrated Antennas for Beam Manipulation Applications: The Two Decades of Progress

BASHAR A. F. ESMAIL[1], (Member, IEEE), SLAWOMIR KOZIEL[1,2], (Fellow, IEEE), LUKASZ GOLUNSKI[2], HUDA BIN A. MAJID[3], (Member, IEEE), AND RUSAN KUMAR BARIK[1], (Member, IEEE)

[1]Department of Engineering, Reykjavik University, 102 Reykjavik, Iceland
[2]Faculty of Electronics, Telecommunications and Informatics, Gdańsk University of Technology, 80-233 Gdańsk, Poland
[3]Fakulti Teknologi Kejuruteraan (FTK), Universiti Tun Hussein Onn Malaysia, Batu Pahat, Johor 84600, Malaysia

Corresponding author: Bashar A. F. Esmail (basharf@ru.is)

This work was supported in part by the Icelandic Centre for Research (RANNIS) under Grant 217771, and in part by the National Science Centre of Poland under Grant 2018/31/B/ST7/02369.

ABSTRACT Metamaterials (MMs) are synthetic composite structures with superior properties not found in naturally occurring materials. MMs have gained massive attention over the last two decades because of their extraordinary properties, such as negative permittivity and permeability. These materials enable many applications in communication subsystems, especially in the field of antenna design, to enhance gain, bandwidth, and efficiency, reduce the size, and deflect the radiation pattern. The demand for beam-deflection antennas is significant in modern wireless communication research studies due to their importance in enhancing service quality, system security, avoiding interference, and economizing power. The MM structures are usually included in the vicinity of the radiating element or incorporated in the antenna substrate for controlling the radiation pattern. This review study provides an introduction to MMs, focusing on their electromagnetic properties, classification, and design approaches. Furthermore, a detailed study of using the MMs to manipulate the radiation is carried out, where different properties such as the positive/negative refractive index, epsilon-near-zero (ENZ), and mu near-zero (MNZ) are employed to achieve a beam-deflection antenna. Reconfigurable MMs are also loaded to the antenna to achieve multi-directional beam deflection with negligible effect on the antenna's physical size. Moreover, the gradient-index (GRIN) based on MMs is used to obtain high deflection angles with minor effects on other antenna properties.

INDEX TERMS Beam deflection, gradient-index (GRIN), metamaterials (MMs), reconfigurable MMs.

I. INTRODUCTION

Metamaterials (MMs) are synthetic composite structures that attracted significant interest over the last two decades due to their peculiar electromagnetic characteristics, such as negative permittivity and permeability [1], [2]. These structures are formed as periodic unit cells whose average size is considerably smaller than the operating wavelength. Their irregular electromagnetic response, the negative permittivity and permeability, was theoretically predicted by Veselago in 1968 [3]. Three decades later, Penury *et al.* proposed the effective medium theory to enable the construction of such materials [4], [5]. The first MM structure, which comprises split-ring resonators (SRR) and metallic wires, was experimentally verified by Smith *et al.* in 2000 [6]. These unique characteristics of MMs enable many practical applications, including super-lense [7], [8] and cloaking technology [9], [10]. Furthermore, they are widely utilized to realize different electromagnetic devices such as filters, absorbers, and sensors [11]–[13].

With the rapid development of wireless communications and radar systems, antennas are required to be multifunctional, low profile, and cheap to fabricate. These requirements are difficult to be fulfilled using a conventional

The associate editor coordinating the review of this manuscript and approving it for publication was Giorgio Montisci.

single-function antenna. Multi-functionality can be obtained by increasing the number of antennas; however, this increases the area occupied by the structure inside the integrated system, thereby increasing the system's size, cost, and weight. Reconfigurable antennas can change their performance characteristics (resonant frequency, radiation pattern, polarization, etc.), thereby constituting promising candidates for realization of intelligent RF frontends. By adjusting the radiated fields of the effective aperture, the currents are redistributed, resulting in a change in antenna functionalities [14], [15]. This empowers the designers to introduce reconfigurable antennas for various communications platforms [16], [17]. Many studies have been carried out on different types of reconfiguration, including the frequency, radiation pattern, directivity, and polarization [18]–[22].

Advances in MMs enabled their new applications in communication subsystems, especially in the antenna field. The unusual electromagnetic properties of these composite structures can be used to improve the performance of a broad range of antennas in terms of directivity, gain, bandwidth, and efficiency, reduction of the physical size, and reconfiguring the radiation beam [23]–[28]. In this work, a particular emphasis will be put on reconfiguring antenna radiation patterns based on the diverse properties of MMs. In modern communication systems, high gain antennas with the beam steering capability are usually preferred, whether installed on terrestrial sites or based on satellites. The millimeter-wave bands such as 28 GHz, 38 GHz, and 60 GHz have recently acquired considerable attention owing to their advantage of providing higher data rate transmissions, which are proposed in the context of the 5G technology [29]. However, these frequencies provide short-range communications due to their high propagation loss. The employment of directional high-gain antennas is an effective and low-cost approach to compensate this loss and increase the communications range at these bands [30], [31]. Nevertheless, the narrow beamwidth that makes beam alignment difficult for the high gain antennas is a significant concern, especially with the movable transmitter or receiver. Redirecting the radiation pattern toward the desired direction provides a solution to revoke this issue. In this regard, MMs are strong candidates to realize 5G antennas of required characteristics. In the literature, various approaches have been proposed for manipulating the antenna radiation characteristics, such as the electrical [32], [33], optical [34], [35], and mechanical methods [36], [37], integrated lens antennas [38], [39], and using the phased array antenna-based phase shifters [40], [41], the traveling wave antennas [42], [43], the beam-forming network (BFN) like the butler matrix [44], [45], and artificial materials, including Frequency Selective Surface (FSS) [46]–[48], Metasurface [49]–[51], Artificial Magnetic Conductor (AMC) [52],[53], Electromagnetic Band-Gap (EBG) [54]–[56], and MMs [57], [58].

Few reviews of the methods for controlling radiation patterns were reported in the literature thus far [59]–[64]. In [59], [60], the authors reviewed the general methods for demonstrating the pattern reconfiguration by focusing on the electrical approach based on switching devices. The radiation pattern manipulation of antennas based on conventional techniques was discussed in [61] and [62], at millimeter-wave and terahertz regimes, respectively. Furthermore, the use of artificial materials based on EBG and metasurfaces was discussed in [63], [64]. Unlike the reported ones, this review investigates the utilized methods for implementing beam deflection antennas based on MMs in the light of the available literature. This review paper discusses the use of different properties of MMs such as positive/negative refractive index, epsilon-near-zero (ENZ), and mu near-zero (MNZ) for achieving beam deflection antennas. Moreover, the reconfigurable MMs were also employed for the same purpose, where the beam deflection in multi-direction can be obtained by utilizing the switching devices. Further, the GRIN lens-based MMs were used to manipulate antenna radiation patterns. The proper design of these media can lead to achieving high deflection angles without affecting other antenna features.

This paper is organized as follows. The electromagnetic properties of MMs, along with their classification and design approaches are discussed in Section II. Section III reviews the various techniques to realize reconfigurable MMs and discusses their applications. The concept of GRIN lens based on MMs is introduced in Section IV. A detailed study of the beam deflection antennas based on MMs is presented in Section V, where different properties of MMs, such as positive/negative refractive index, epsilon-near-zero (ENZ), mu near-zero (MNZ), the reconfigurable MMs, and the GRIN lenses are utilized for controlling the radiation pattern. The challenges and future research directions are discussed in Section VI. Section VII concludes the paper.

II. MMS ELECTROMAGNETIC BEHAVIOR AND THEIR CLASSIFICATION

Although MMs are complex structures, their electromagnetic properties are determined through Maxwell's equations, which can assist in demonstrating the features of MMs. Maxwell's equations are given by [65], [66]

$$\nabla \times \vec{E} = -\frac{\partial \vec{B}}{\partial t} - \vec{M} \tag{1}$$

$$\nabla \times \vec{H} = \vec{J} + \frac{\partial \vec{D}}{\partial t} \tag{2}$$

$$\nabla \cdot \vec{D} = \rho_e, \quad \nabla \cdot \vec{B} = \rho_m \tag{3}$$

where $\vec{E}(\vec{H})$ is the electric (magnetic) field vector, $\vec{D}(\vec{B})$ is the displacement of electric (magnetic) flux density vectors, $\vec{J}(\vec{M})$ is the electric (magnetic) current density vector, and $\rho_e(\rho_m)$ is the scalar electric (magnetic) charge density. The constitutive relations are used to fully depict the interaction of the electromagnetic fields, which are given by $\vec{D} = \varepsilon\vec{E}$ and $\vec{B} = \mu\vec{H}$. The jω can be used to represent the time derivatives in (1) and (2), where the time dependence is assumed to be of the form $e^{j\omega t}$. Here, the Maxwell's equations can be

expressed as

$$\nabla \times \vec{E} = -j\omega\mu\vec{H} - \vec{M} \quad (4)$$
$$\nabla \times \vec{H} = j\omega\varepsilon\vec{E} + \vec{J} \quad (5)$$

where $\varepsilon(\mu)$ is the permittivity (permeability). Equations (4) and (5) can be presented without sources, electric and magnetic current densities:

$$\vec{k} \times \vec{E} = \omega\mu\vec{H} \quad (6)$$
$$\vec{k} \times \vec{H} = -\omega\varepsilon\vec{E} \quad (7)$$

where $\vec{k}$ is the wave vector. Additionally, the Poynting power, $\vec{S}$, can be used to assess the characteristics of materials, in which the real part is used to demonstrate the energy flow [67]. The $\vec{S}$ vector has the form of $\vec{S} = 0.5(\vec{E} \times \vec{H}^*)$. It is known that both ε and μ are positive in the homogeneous medium, in which the $\vec{E}, \vec{H}$, and $\vec{k}$ follow the right-hand rule. Therefore, they are called right-handed materials (RHMs). In this case, the $\vec{S}$ and $\vec{k}$ have the same direction, as illustrated in top-right quarter of Fig. 1. When $\varepsilon < 0$ and $\mu < 0$, the $\vec{E}, \vec{H}$, and $\vec{k}$ follow the left-hand rule, and the medium here is the left-handed materials (LHMs) or MMs [68]. In such materials, the $\vec{S}$ and $\vec{k}$ are antiparallel, as shown in the bottom-left quarter of Fig 1. LHMs support backward-wave propagation, where the phase velocity and group velocity are antiparallel.

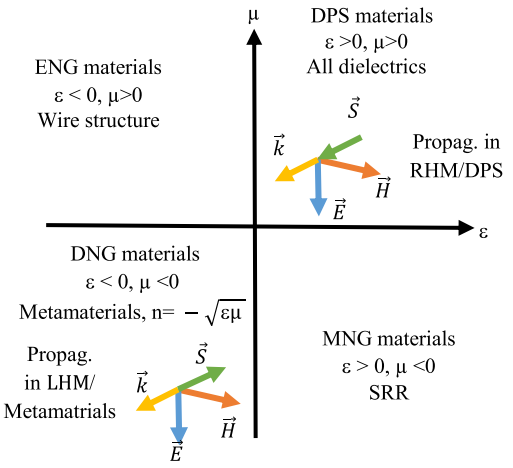

FIGURE 1. Classifications of the materials based on the signs of the ε and μ and the propagation in the RHM/DPS and LHM/Metamaterials.

The classification of MMs is contingent upon the signs of the two fundamental quantities of material; ε and μ. As claimed by Veselago, some unusual phenomena occur in these materials, such as reversed Snell Law, Cerenkov radiation, and Doppler shift [69]–[71]. Figure 1 shows the material classifications based on ε and μ with the electromagnetic wave interacting with four possible materials. The top-right quarter of Fig. 1 shows the double-positive (DPS) materials with $\varepsilon > 0$ and $\mu > 0$. This type includes the majority of classic dielectric materials. The top-left quarter presents the epsilon negative (ENG) material. This type induces negative ε at some frequencies and positive μ at all frequencies, which is realized by periodic wire structures [72]. The mu-negative (MNG) material is realized by a periodic structure of split-ring resonators (SRRs), which is presented in the bottom-right quarter [6]. The most interesting one is located at the bottom-left quarter, in which ε and μ are simultaneously negative. This type is known as double-negative materials (DNG)/MMs, which cannot be found naturally.

III. RECONFIGURABLE MMS

Over the last two decades, MMs have been used to construct many novel devices. Their limitations, such as the narrow bandwidth and the losses, can be alleviated by embedding several reconfigurable techniques at the cost of increasing the fabrication complexity and expense. Reconfigurable MM is defined as modifying the electromagnetic response of such structures purposely as a part of the ordinary operation of the device through the change of geometry or material properties. Modern advancements in reconfigurable MMs have increased the possibility of fabricating unique subwavelength ($< \lambda/4$) devices with practical functionality [73], [74]. In the literature, various MM structures are reconfigured for diverse purposes at different frequency bands; microwave, millimeter-wave, and terahertz [75]–[82]. Several reconfigurable methods were proposed to create dynamic changes in MMs characteristics, including mechanical, thermal, and electronic. The MMs can be reconfigured mechanically by adjusting the distance between their elements or between the MMs and the substrate, thereby altering the resonance response. However, this method increases the complexity and the fabrication cost [83], [84]. On the other hand, the electromagnetic response of many material characteristics, such as a refractive index, undergoes a change when variable temperatures are applied. Therefore, MMs can be reconfigured thermally by altering their response using an external temperature adjustment [85]. Nevertheless, many tunable devices are operated at the room temperature, and this approach may not be suitable for real-world applications. The electronic approach has gained considerable attention because of its capability to modify MMs' electromagnetic response using different active switches. The development of both electronics and semiconductor industries empowers the combination of active switching components such as a varactor diode, PIN diode, and Micro-electro-mechanical systems (MEMS) with printed circuits. A varactor diode is modeled as a variable capacitance that external bias voltages can control [86], [87]. It represents the most common tuning method because of its simple integration into many MM shapes and the ease of biasing because of using only a single diode to realize the reconfiguration. However, low sensitivity of the capacitance changes limits the tuning range of such a device. On the other hand, the PIN diode is represented by a variable resistance controlled by an external voltage. Both PIN and varactor diodes can be used in MMs for the same purposes [88]–[91]. The MEMS switches offer many benefits over alternative solutions, such as switching capability with high efficiency and isolation, as well as moderate losses [92]–[94].

Nevertheless, high operating voltages, manufacturing cost, and slow switching speed are the main shortcomings limiting their use as RF switches in MMs [73]. It is worth mentioning that there are other methods to reconfigure the MMs, such as including the graphene into the substrate of the unit cell and controlling its response by applying different chemical potentials [95]. Controlling of the electromagnetic response of the MMs enables their use in a wide variety of applications, including:

- Reconfigurable filters and antennas; here, the focus is on MMs that are principally designed to tune the resonant response or alter bandwidth 95]–[97];
- Optimized scattering (transmission, reflection, and absorption) of materials at the desired resonant frequency [86], [87], [98].
- Manipulation of wave propagation characteristics such as directivity, gain, and radiation beam [99], [100].

A detailed review of applications of reconfigurable MMs in beam deflection antennas will be presented in Section V.

IV. GRADIENT-INDEX (GRIN) MMS

GRIN lenses received significant attention owing to their ability to focus the radiation. These lenses were proposed as alternatives to the established dielectric counterparts. The homogeneous MMs can be obtained using congruent unit cells arranged in an array form, which are employed in a wide range of applications. On the other hand, if unit cells vary in size, the medium is called inhomogeneous, GRIN, which enables unusual microwave or optical response [101]. The refractive index distribution can be realized based on MMs, which is achieved by the geometric tailoring of the neighboring unit cells. The GRIN based on MMs was proposed theoretically and verified experimentally in [102]–[104], in which the conventional SRR was used as a resonance structure to build a giant inhomogeneous medium. The inherent non-resonant and low-loss behaviors of GRINs enable many practical applications that include but are not limited to the realization of the traditional Luneburg lens [105], [106], and the radar-absorbing system [107], as well as increasing the quantum of energy transfer [108]. Further, this medium can mutate the spherical wave to the planar wave. Thus, the antenna characteristics such as gain, directivity, beamwidth, and sidelobe level can be improved [109]–[111]. The most significant application of the GRINs in the field of antennas is controlling the electromagnetic wave propagation [112]–[114]. The use of GRINs to guide the radiated beam of antennas into pre-defined directions is discussed in Section V.

V. ANTENNA LOADED MMS FOR BEAM DEFLECTION APPLICATION

The radiation pattern is one of the most crucial performance figures of antennas. In some applications, such as wireless base stations, satellite communications, and radar systems, the antennas with beam deflection capability are instrumental as they are able to enhance the performance in terms of system security, avoiding interference, and economizing power. In the literature, MMs were proposed in the last decade for beam tilting applications, which are considered one of the best approaches due to their adjustable refractive index, simplicity of implementation, low profile structure, and potential for integration onto the same substrate, the antenna is implemented on. These artificial materials are placed close to the radiating elements or etched in the same substrate to manipulate the radiation pattern. A detailed review of different beam deflection approaches based on MMs is conducted in this section.

A. BEAM DEFLECTION ANTENNA BASED ON AN ARRAY OF MMs

The MMs are incorporated into various antennas to manipulate the radiation pattern, arranged in the proximity of the radiating part or etched on the substrate. The array of MM is inserted in the path of electromagnetic waves emitting from the radiating element, guiding them toward the desired direction. In this subsection, an array of MMs for performing the beam deflection antennas at different frequency bands is reviewed and discussed, in which several properties were used, such as the positive/negative refractive index, epsilon-near-zero (ENZ), and mu near-zero (MNZ) [27], [57], [58], [115]–[130].

The microwave regime is the most studied part across the spectra for demonstrating the beam deflection antennas using various MM structures. This is due to the availability of the materials and equipment for fabrication and measurement in most laboratories [27], [57], [58], [115]–[124]. The beam deflection mechanism of end-fire antennas depends on the media having different refractive indices, placed in the path of the electromagnetic waves [57], [115]. The simplest way to create a diverse refractive index medium on the limited area of the substrate is by designing suitable MMs. Here, the MM array and the antenna substrate are employed to create different refractive index sections in the path of the electromagnetic waves that undergo a phase change and are then deflected toward the desired direction. The benefits of the MMs are to provide a higher refractive index than that of the substrate and maintain the antenna's size by incorporating them directly into the substrate. Figure 2 presents two media with different refractive indices incorporated in the vicinity of the electromagnetic source, where n and φ are the refractive index and deflection angle, respectively. $L(d)$ is the length (width) of the mediums. β_1 and β_2 are the phassbased on the refractive index of the twomediums. The phase difference is given by $\Delta\beta = k_0(n_2 - n_1)d$. The relation between β and the beam deflection angle φ is given by $\beta = k_0 L \sin\varphi$. The beam deflection angle can be predicted theoretically using the following expression.

$$\varphi = sin^{-1}\left[\frac{d(n_2 - n_1)}{L}\right] \tag{8}$$

In [115], 3×4 unit cells of an H-shaped resonator were inserted into the bow-tie antenna substrate for tilting the

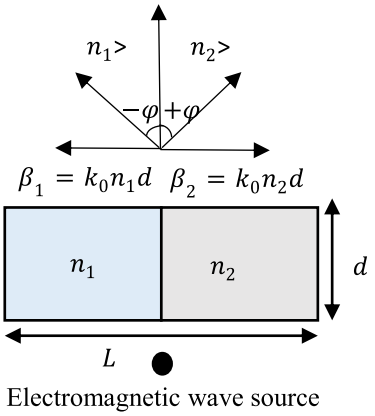

FIGURE 2. The mechanism for the beam deflection for the end-fire antenna based on the MM array.

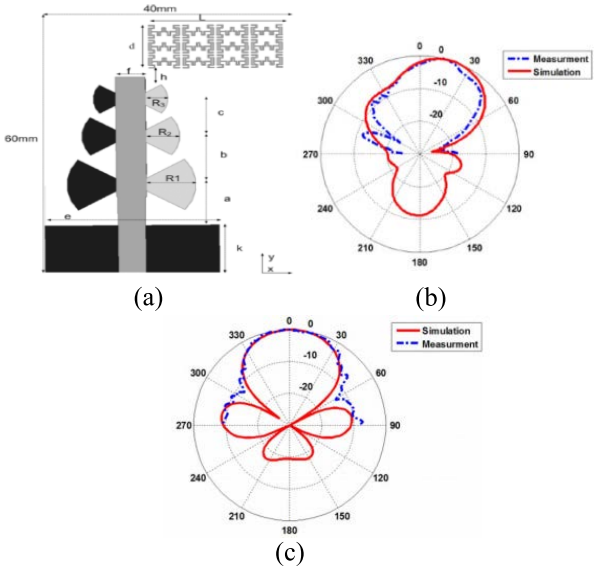

FIGURE 3. The bow-tie antenna of [115] with an array of H-shaped resonators: (a) the configuration of MM antenna, the simulated and measured radiation patterns at 7.5 GHz in (b) E-plane and (c) H-plane.

radiation angle in the E-plane at a C-band. The MM array was shifted from the center of the antenna to the right to create a region with different refractive indices in the path of electromagnetic waves. The configuration of the proposed antenna, including the H-shaped unit cells, is presented in Fig. 3(a). Deflection angle of 17° was obtained with a gain enhancement of 2.73 dB at 7.5 GHz, as displayed in Fig. 3(b). According to (8), the deflection angle is determined by the difference in the refractive index of the two media (MM array and antenna substrate) and the dimensions of the MM array. By applying the values of L = 21.5 mm, d = 9.7 mm, $n_2 = 2.2$ and $n_1 = 1.6$ in (8), the deflection angle $\varphi = 17°$ was obtained. Figure 3(c) shows no deflection in H-plane as expected as the MM array was incorporated in the E-plane only. The same mechanism was applied by Esmail *et al.* in [57]. The radiation beam of a dipole antenna was deflected by angles of 25° and −24° with gain enhancements of 3 dB and 2.7 dB, respectively, at a sub-6 GHz band of 3.5 GHz. This study demonstrates high deflection angles with good gain improvement. Equation (8) was modified to incorporate more parameters for calculating the deflection angle as follows:

$$\varphi = sin^{-1}\left[\frac{d(n_2 - n_1)}{L\sqrt{(\varepsilon_r + 1)/2}}\right] \tag{9}$$

The relative permittivity of the substrate is included for a better prediction of deflection angle besides the dimensions and refractive indices of the MMs array and the substrate. By applying the values of L= 59.5 mm, d= 51 mm, $n_2 = 2$, $n_1 = 1.4$, and $\varepsilon_r = 2.2$ in (9), the positive deflection angle $\varphi = 25°$ was obtained. The negative deflection angle can be achieved by reversing the values of the refractive indices. Also, at sub-6 GHz, the beam deflection was demonstrated using a 5 × 4 array of double G-shaped resonators (DGRs) placed vertically on the substrate in the elevation plane [116]. The radiation beam was deflected by 35° in H-plane with the gain improvement of 5 dB at 3.6 GHz.

The transformation optics proposed by Pendry *et al.* in 2006 [131] give the ability to control electromagnetic wave by transferring it from one space to another. The basic idea is that the Maxwell equations remain form-invariant under coordinate transformations. The result of a particular transformation is a direct link between the permittivity and permeability of the material in different coordinate systems. Several novel transformation optics-based devices have been investigated over the last two decades, such as invisibility cloaks [132], wave rotating [133], and flat reflectors [134]. On the other hand, the authors in [135] demonstrated that two adjacent slabs with the same thickness and opposite signs of the constitutive parameters could act as a zero thickness medium. Here, when a specific volume of space folds to the other one, the corresponding boundaries have identical fields under all circumstances. Therefore, the combination of the transformation optics and folded geometry has led to the construction of many novel devices such as external cloak [136] and EM concentrator [137]. Recently, this approach was used to control electromagnetic waves [58]. Barati *et al.* [58] merged the conventional SRR and a meander line to form a unit cell for tilting the radiation beam of the patch antenna array. The MMs are arranged in a triangular shape, and placed vertically above the antenna array. The mechanism of beam deflection is based on folded transformation optics. The fabricated patch antenna array and antenna with MMs are displayed in Figs. 4(a) and (b), respectively. The radiation beam was deflected by 15° at 7.3 GHz, as shown in Figs. 4(c) and (d). However, the gain was reduced by 1.5 dB. This degradation is due to the employing of patch antenna as a source that has a wavefront with curved top surfaces. The patch wavefront can be represented by an infinite number of plane waves with different incident angles. Therefore, for each incident plane wave, the Poynting vector refraction angle will differ in the physical domain, causing

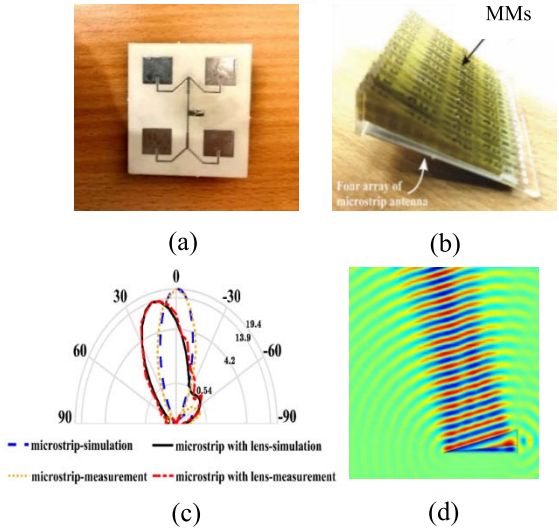

FIGURE 4. The beam deflection system based of [58]: (a) the fabricated patch antenna array, (b) the photograph of the fabricated MM patch array, (c) the simulated and measured radiation patterns with and without MMs at 7.3 GHz, and (d) the electric near-field distribution.

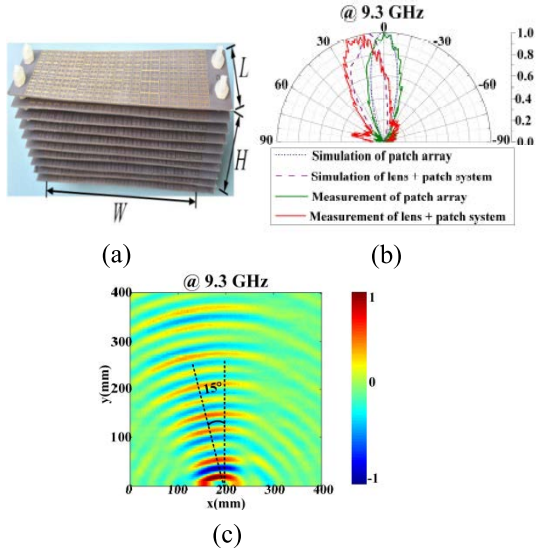

FIGURE 5. The beam deflection system based of [119]: (a) photograph of the fabricated MMs lens, (b) simulated and measured radiation pattern in the broadside direction of the patch array with and without MMs lens, and (c) the measured electric near-field distribution at 9.3 GHz.

power distribution to deviate from its predefined angle and radiate in other directions. Thus, the main lobe amplitude will be decreased to satisfy the conservation law of energy, which leads to a decrease in the gain. The beam tilting antenna based on phase varying of MMs was implemented in [117], [118]. In [117], the MM unit cell consists of capacitive and inductive grids, in which the phase varying MM was created by controlling the gaps between the metallic strips of the capacitive grid. The MM array was mounted above the patch antenna, where the E-plane radiation pattern was deflected in both directions by angles of ±20° at 10 GHz. On the other hand, the varying phase was implemented by adjusting the inductive grid and fixing the capacitive grid [118]. By mounting these structures above the patch antenna, the radiated beam was deflected by 56° in the broadside direction at 10 GHz. Jianjia *et al.* [119] proposed MM based on an electric-LC resonator (ELC) to control the patch antenna's radiation pattern. 5 × 20 ELC unit cells were arranged in ten layers to form a lens, and fed by a patch antenna, as illustrated in Fig. 5(a). Figures 5(b) and (c) show that the radiated beam is deflected by 15° at 9.3 GHz. However, this arrangement leads to an increase in the overall size of the beam deflection system. The reconfigurable radiation pattern in both positive and negative directions was implemented by Le *et al.* in [120]. One layer of 5 × 17 folded-line left-handed (FL-LHM) unit cells was located above the patch antenna for tilting the radiated beam by ±20° with a gain enhancement of 3 dBi at 5.8 GHz. Li *et al.* [121], introduced NRIM as a phase shifter in the leaky-wave antenna array feeding line for steering the radiated beam by 66° (58°−124°) in E-plane at 2.4 GHz. Also, in [122], the NRIMs were integrated with the dielectric resonator antenna (DRA) for obtaining positive and negative deflection angles at C-band. By building four layers of the fractal cross ring resonator over the two DRA antennas, the main beam was tilted by angles of ±38° in E-plane with a gain enhancement of 1 dB over 5−5.5 GHz. The photograph of the proposed antenna with MM layers is shown in Fig. 6(a). The measured radiation patterns of the antenna with and without MM layers in both E-plane and H-plane at 5.2 GHz are depicted in Figs. 6(b) and (c). Here, the positive and negative deflections were obtained by changing the excitation ports of the two DRAs. The beam deflection mechanism was explained based on the Snell's law,

$$sin\theta_1.n_{air} = sin\theta_2.n_{MMs} \tag{10}$$

where the θ_1 (θ_2) is the incident angle of the electrometric wave from the air to the MM array (from the MM array to air). The n_{air} (n_{MMs}) is the refractive index of the air (MM array). The θ_1 is decided by l and d, as illustrated in Fig. 6(d). Based on Fig. 6(d) and the values of $n_{MMs} = 1.4$, $l = 25$, $d = 14$ the calculated deflection angle is 38.5°, which agrees with the simulated and measured results. Dual-band beam tilting antennas based on MMs in E-plane and H-plane were reported in [123] and [124], respectively. Two different unit cells, meander-line and H-shape, were etched on both sides of a bow-tie antenna, in which they were shifted from the center of the antenna to provide beam deflection angles of 17° and −20° in E-plane at 2.4 GHz and 5.5 GHz, respectively [123]. Moreover, the gain was magnified by 1.5 dBi at 2.4 GHz and 2.7 dBi at 5.5 GHz. The fabricated prototype of the proposed antenna with two MM structures is presented in Fig. 7(a). Figures 7(b) and (c) depict the deflection angles in the E-plane. The beam deflection was achieved by integrating a greater refractive index media in the off-axis of the end-fire antenna. The waves travel a short path through the MMs area denoted by "a", and a long path, $b = \sqrt{L^2 + a^2}$, through the

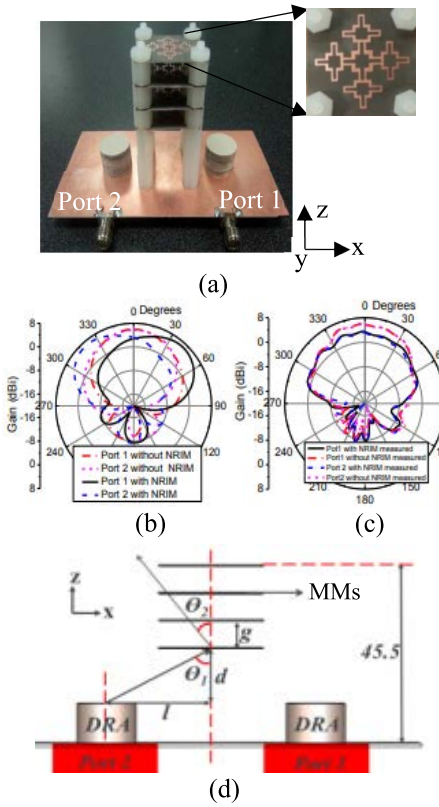

FIGURE 6. The DRA array of [122] with NRIMs: (a) fabricated DRA array with four MM layers. The inset shows the fabricated prototype of the fractal cross ring resonator, (b), (c) the measured radiation patterns of the proposed antenna with and without NRIM in E-plane and H-plane, respectively, when different ports are excited at 5.2 GHz, and (d) the mechanism of the beam deflection.

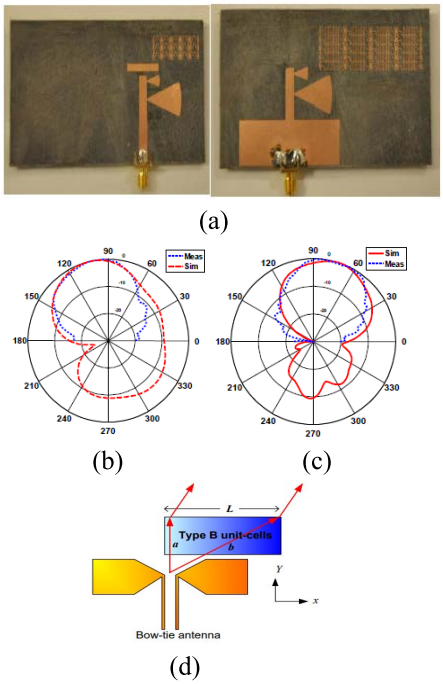

FIGURE 7. The bow-tie antenna of [123] with two MM structures: (a) front and back views of fabricated bow-tie antenna with H-shape and meander line unit cells, the simulated and measured radiation patterns in E-plane (b) at 2.4 GHz, and (c) at 5.5 GHz, and (d) the mechanism of the beam tilting.

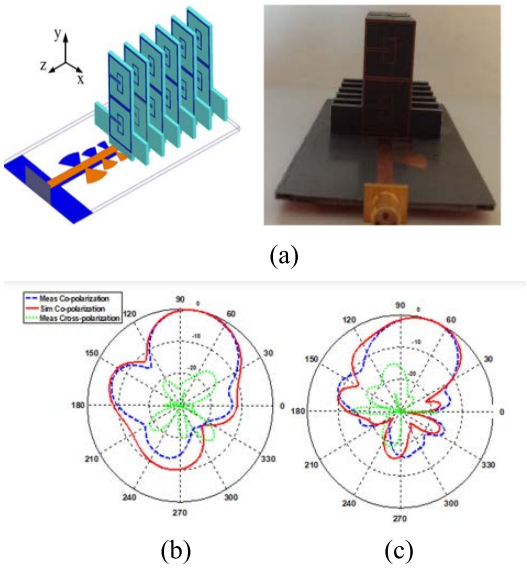

FIGURE 8. The bow-tie antenna of [124] with DSRs: (a) the configuration and fabricated prototype of the MM antenna, the simulated and measured radiation patterns in H-plane at (b) 3.5 GHz, and (c) 5.5 GHz.

MMs area denoted by "b", as shown in Fig. 7(d). where L is the length of MMs in the x-direction. The beam deflection is due to the phase difference resulting from electromagnetic rays passing through two media of different refractive indices (MMs and antenna substrate). Therefore, simply increasing the length of the MMs along the x-direction results in a larger phase differential and consequently causes a larger deflection angle. Further, the same research group proposed a 2×6 arrangement of double split rectangular (DSR) unit cells located vertically on the antenna substrate to achieve beam deflection angles of 17° and 20° in H-pane at 3.5 GHz and 5.5 GHz, respectively [124]. The gain enhancements of 4.7 dBi and 5.5 dBi at 3.5 GHz and 5.5 GHz, respectively, were observed when the MM unit cells were arranged symmetrically in the H-plane. The antenna with the DSR unit cells is presented in Fig. 8(a), whereas the obtained deflection angles at both frequencies in H-plane are displayed in Figs. 8(b) and (c).

Recently, the millimeter-wave band has gained growing interest and now appears to be the most likely candidate to deliver the wireless multi-gigabit applications for 5G wireless networks and beyond. This band is expected to present a large bandwidth to meet higher data rate transmissions demand. However, these frequencies suffer from high propagation loss due to the short wavelength, only allowing short-range communications. High-gain antennas with beam deflection capability constitute an effective and low-cost approach to increase the communication range and provide better beam alignment at this band [138], [139]. MMs are strong candidates to realize millimeter-wave antennas of required characteristics. In the literature, different MM structures were

used to deflect the radiation pattern of various millimeter-wave antennas [125]–[130]. The radiated beam of the horn antenna was steered by ±15° at 144 GHz using ε near-zero (ENZ) MM [125]. The ENZs act as a lens realized by hollow rectangular waveguides arranged in an array form at the horn antenna aperture. Low permeability based on SRR was implemented in [126] to deflect the bow-tie antenna's radiation beam by 22° in H-plane with gain augmentation of 6 dBi at 60 GHz. The beam tilting of a dipole antenna was achieved by Dadgarpour *et al.* [127] using high refractive-index modified H-shape unit cells. Four slabs of H-shape were installed vertically in the elevation plane of the antenna for performing beam tilting of 30° in the H-plane over 57–64 GHz. Esmail *et al.* [128] proposed 3 × 3 square range resonators (SRRs) embedded in the dipole antenna substrate to obtain the deflection in both directions. The E-plane radiation pattern was deflected by angles of 24° and −25° with gain improvements of 1.87 dB and 1.84 dB, respectively, at 28 GHz. The beam deflection in both azimuth and elevation planes was implemented using MNZ and ENZ in [129] and [130], respectively. The radiation pattern of the double feed dipole antenna was deflected in E-plane by loading ten slabs of MNZ unit cells vertically on antenna substrate, where two slabs included 6 × 4 unit cells, and eight slabs comprised 10 × 4 unit cells, as presented in Fig. 9(a) [129]. Figure 9(b) shows that the tilting angles of ±35° were obtained with a gain enhancement of 8 dB at 60 GHz. To obtain E- and H-planes beam deflections, eight slabs of 10 × 7 MNZ unit-cells were positioned in the elevation plane of the four feed dipole antennas, as shown in Fig. 9(c). Figures 9(d) and (e) illustrate that the radiated beam is deflected by 35° in H-plane and −35° in E-plane. The beam deflection is due to electromagnetic waves traversing in two media of different refractive indices as predicted by Snell's law. The MM array acts as a lens to deflect the radiation beam in a predefined direction. To implement this approach, the MM array is shifted from the center of the antenna to provide different refractive indices in the path of the electromagnetic waves. In parallel, three slabs, each with six ENZ unit cells, were located above the slot antennas for reconfiguring the radiation in both planes, as shown in Figs. 10(a) and (b) [130]. The slabs were shifted from the center towards (–x)-direction for performing the H-plane deflection. By exciting port 1 and terminating port 2, a tilting angle of −30° in the H-plane is obtained, as displayed in Fig. 10(c). On the other hand, the deflection angle of −30° was obtained in the E-plane when the slabs were moved from the center towards (–y)-direction, as shown in Fig. 10(c). Table 1 summarizes the beam deflection antenna using an array of MMs.

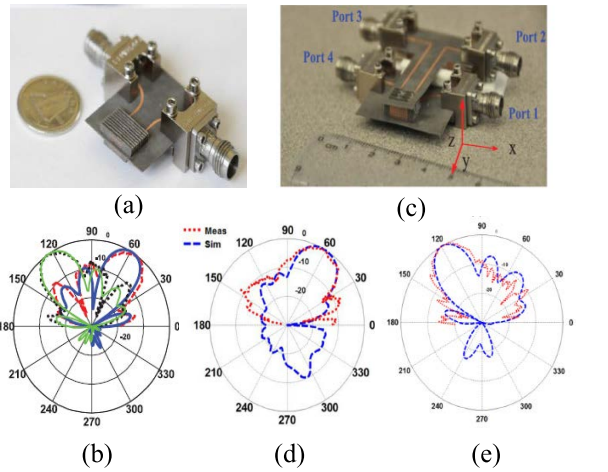

FIGURE 9. The dipole antenna array of [129] with MNZs: (a) the photograph of the double feed dipole antenna with 10 slabs of MNG array: 2 slabs include of 6 × 4 unit cells and 8 slabs include of 10 × 4 unit cells, (b) beam steering angles in the E-plane at 60 GHz, (c) the photograph of four feed dipole antenna with eight slabs of MNG where each slab comprise 10 × 7 unit cells, the simulated and measured deflection angles at 60 GHz (d) in the H-plane, and (e) in the E-plane.

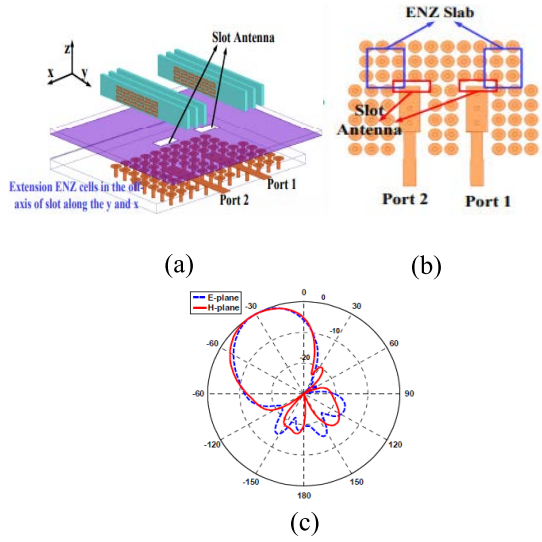

FIGURE 10. The double feed slot antenna with off-center ENZ array based of [130]: (a) side view, (b) top view, and (c) the deflection angles in both the E and H-planes when port1 is excited.

B. RECONFIGURABLE MMS FOR BEAM-DEFLECTION ANTENNA

The reconfigurable property is in high demand to increase the functionalities of the devices and reduce their size. As MMs are used in many devices, the reconfigurable property is essential to developing their performance. This property can be used to deflect the antenna's radiation pattern in multiple directions, in which the size of such a system can be substantially reduced. In this regard, instead of using multiple antennas, the reconfigurable MMs are integrated with the antenna for achieving deflection angles in multi directions. The reconfigurable MMs based PIN diodes for beam deflection applications were proposed in [140]–[145]. The authors in [140], [141], proposed a reconfigurable MMs-based PIN diode for tilting the radiation pattern of dipole antenna at 5G band of 28 GHz. In [140], the E-plane radiation pattern was deflected by 30° and −27° depending on the arrangement of reconfigurable contiguous squares resonator (CSRs)

TABLE 1. Summary of beam deflection antennas using an array of MMs.

Ref.	Antenna type	Frequency band	Beam deflection angle (Plane)	Gain	Efficiency and (bandwidth)	Substrate material	MM structure
[57]	Dipole antenna	S-band (3.5 GHz)	25° and −24° (E-plane)	Increased by 3 dB and 2.7 dB, respectively	— (Not affected)	Rogers RT5880	Adjacent square-shaped resonator (ASSR)
[58]	Patch antenna	C-band (7.3 GHz)	15° (E-plane)	Dropped by 1.5 dB	— (Increased by 20%)	FR-4	SRR and meander line
[115]	Bow-tie antenna	C-band (7.5 GHz)	17° (E-plane)	Increased by 2.73 dB	— (—)	Rogers RT5880	H-shape
[116]	Bow-tie antenna	S-band (3.5 GHz)	35° (H-plane)	Increased up to 5 dB	— (Decreased by 42.8%)	Rogers RT5880	Double G-shaped resonator (DGR)
[117]	Patch antenna	X-band (10 GHz)	±20° (broadside direction)	—	— (—)	FR4	Capacitive and inductive grids composite MM
[118]	Patch antenna	X-band (10 GHz)	56° (broadside direction)	—	90% (—)	FR4	Capacitive and inductive grids composite MM
[119]	Microstrip antenna	X-band (9.3 GHz)	15° (E-plane)	—	— (—)	—	ELC
[120]	Patch antenna array	C-band (5.8 GHz)	±20° (broadside direction)	Increased up to around 2.5–3dBi	— (—)	Rogers RT5880	FL-LHM
[121]	Leaky wave antenna array	S-band (2.4 GHz)	66° (E-plane)	—	— (—)	FR4	1-stage NRI phase shifter
[122]	Dielectric resonator antenna (DRA)	C-band (5-5.5 GHz)	±38°	Increased up to 1 dB	— (Not affected)	Rogers RT5880	Fractal cross ring resonator structure
[123]	Bow-tie antenna	S-band (2.4 GHz) and C-band (5.5 GHz)	17° at 2.4 GHz −20° at 5.5 GHz (E-plane)	Increased by 1.5 dBi at 2.4 GHz and 2.7 dBi at 5.5 GHz	90% (—)	Rogers RT5880	H-shaped meander line
[124]	Bow-tie antenna	S-band (3.5 GHz) and C-band (5.5 GHz)	17° at 3.5 GHz 20° at 5.5 GHz (H-plane)	Increased by 1.5 dBi at 2.4 GHz and 2.7 dBi at 5.5 GHz	— (—)	Rogers RT5880	Double split rectangular (DSR)
[125]	Horn antenna	Millimetre-wave (144 GHz)	±15°	—	— (—)	—	ε-near-zero (ENZ) MM
[126]	Bow-tie antenna	V-band (60 GHz)	22° (H-plane)	Increased up to 6 dBi	— (—)	Rogers RT5870	Low-permeability based SRR MM
[127]	Dipole antenna	V-band (60 GHz)	30° (H-plane)	Increased up to 5 dB	— (—)	Rogers RT5880	Modified H-shaped structure
[128]	Dipole antenna	Ka-band (28 GHz)	24° and −25° (E-plane)	Increased by 1.87 dB and 1.84 dB, respectively	— (Not affected)	Rogers RT5880	SRR
[129]	Dipole antenna	V-band (60 GHz)	▪ ±35° (E-plane) ▪ 35° (E and H-plane, respectively)	-Increased by 8 dB (E- and H planes)	88% (—)	Rogers RT5870	Capacitively-loaded loop (CLL) structure
[130]	Slot antenna	V-band (60 GHz)	−35° (E and H-plane, respectively)	Increased by 5.3 dB	— (—)	Rogers RT5880	Meander-line H-shape

on the antenna substrate, as shown in Figs. 11(a) and (b), respectively. In addition, the gain is improved by 1.9 dB and 1.5 dB for the positive and negative deflections, respectively. Three switches were used to reconfigure the MM structure, in which only two states (ON and OFF) were studied to exhibit different refractive indexes in the way of electromagnetic rays. The ideal switches based on copper strips were used as a proof of concept. The theoretical concept of radiation beam deflection relies on two MM configurations of different refractive indices placed in the way of the

electromagnetic rays, cf. Figs. 11(c) and (d). In Fig 11(c), 2 × 3 unit cells of reconfigurable MM were inserted in the front of the dipole antenna with overall dimensions of 9.9 mm × 6.4 mm. Two rays of the electromagnetic wave (emitted from source o) travel over the reconfigurable MM and reach two points; m1 (ON state) and m2 (OFF state). The position of all elements in the coordinate plane is revealed in Fig 11(d). The calculation of the array factor (AF) at far-field is used to determine the resultant effect of each ray. The AF can be expressed as

$$AF = 1 + e^{ikd_1 cos\gamma_1} + e^{ikd_2 cos\gamma_2} \tag{11}$$

where k and d are the wavenumber and the ray length, respectively. The unit vectors $\hat{a}_{m1o}$ and $\hat{a}_{m2o}$ that extends from the feed point o to the two MM configurations are given by

$$\begin{aligned} \hat{a}_{m1o} &= 0.61\hat{a}_x + 0.79\hat{a}_y, \quad \text{and} \\ \hat{a}_{m2o} &= -0.33\hat{a}_x + 0.94\hat{a}_y \end{aligned} \tag{12}$$

The two electromagnetic rays induce angles of γ_1 and γ_2 with the unit vector of the coordinate plane. The angles γ_1 and γ_2 are obtained by the dot product of unit vector $\hat{a}_{ro}$ with $\hat{a}_{m1o}$ and $\hat{a}_{m2o}$, respectively. At $\theta = 90°$ plane and $\varphi \in (0, 360°)$, the γ_1 and γ_2 are calculated as follows;

$$\begin{aligned} \cos\gamma_1 &= 0.61cos\varphi + 0.79sin\varphi, \quad \text{and} \\ \cos\gamma_2 &= -0.33cos\varphi + 0.94sin\varphi \end{aligned} \tag{13}$$

The radiation pattern is determined by multiplying the AF and the dipole antenna element factor $(cos((\pi/2)\cos\varphi)/sin\varphi)$ [146], which can be expressed as follows:

$$\begin{aligned} \text{Radiation pattern} = &\left(1 + e^{ikd_1\cos\gamma_1} + e^{ikd_2\cos\gamma_2}\right) \\ &\times \cos((\pi/2)\cos\varphi)/sin\varphi) \end{aligned} \tag{14}$$

In parallel, four switches were used to reconfigure the MM structure in [141], in which the beam was deflected by angles of 34° and −31° with gain enhancements of 1.7 dB and 1.5 dB, respectively. The authors applied the same beam deflection mechanism as in [140]. Two capacitively-loaded loop (CLL) rings with one switch on each were located on the monopole antenna substrate for tilting the radiation beam by angles of 90° and 270° at 1.18 GHz [142]. The first deflection angle was obtained by enabling one switch with ON state and another with OFF state, whereas the second angle was achieved when both switches were OFF. Figures 12(a) and (b) depict the MM antenna's configuration and measured radiation patterns in the E-plane, respectively. In [143], the same research group used two, three, and four SRRs arranged around the monopole antenna for achieving two, three, and four deflection angles, respectively, where one switch was placed in each SRR. Yan *et al.* [144] proposed three MM unit cells with two diodes to reconfigure the wearable patch antenna at 2.4 GHz. The antenna operated as a conventional patch with a patch-like radiation pattern (broadside radiation pattern) when the diodes were OFF, while it provided a monopole-like radiation pattern if the diodes were ON (omnidirectional radiation pattern). The conventional SRR was

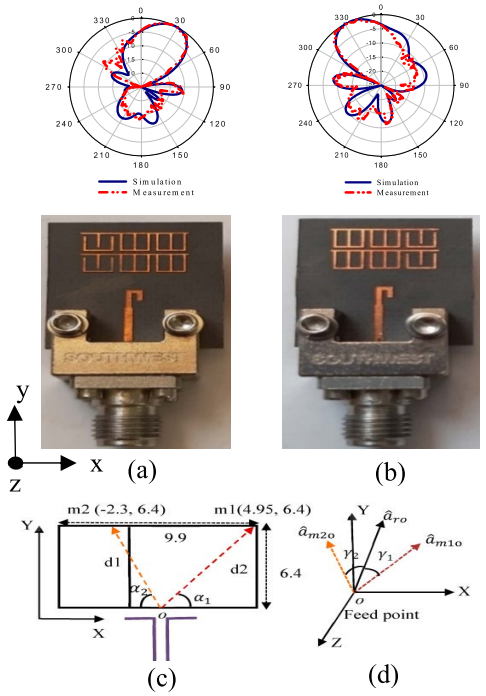

FIGURE 11. The dipole antenna with an array of reconfigurable MMs based of [140]: (a) positive beam deflection and (b) negative beam deflection, and the mechanism of beam deflection; the electromagnetic ray routes and their locations from the feed point for array factor and radiation pattern calculations (c) on the structure and (d) on the coordinate plane.

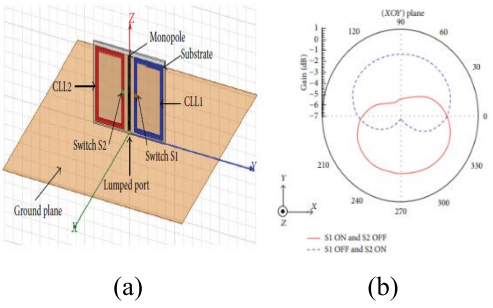

FIGURE 12. Monopole antenna with two CLL rings based of [142]: (a) the configuration of MM antenna, and (b) the measured radiation patterns in E-plane according to the states of the switches.

reconfigured based on three PIN diodes and used to tilt the dipole antenna radiation pattern [145]. Two configurations of SRR were obtained based on the state of the three PIN diodes, as shown in Fig. 13(a). The first configuration was obtained when the D1 and D3 were ON and D2 was OFF. The second configuration was achieved by putting the D2 to ON and D1 and D3 to OFF. The ideal switches based on copper strips were used as a proof of concept. As illustrated in Figs. 13(b) and (c), the reconfigurable SRRs (two configurations) were included in the same antenna substrate to obtain a tilting angle of 32° in the E-plane at 60 GHz. There is no deflection in the H-plane as expected [Fig. 13(d)]. In addition, this beam deflection is accompanied by a gain enhancement of 2.4 dB. The two configurations create different refractive

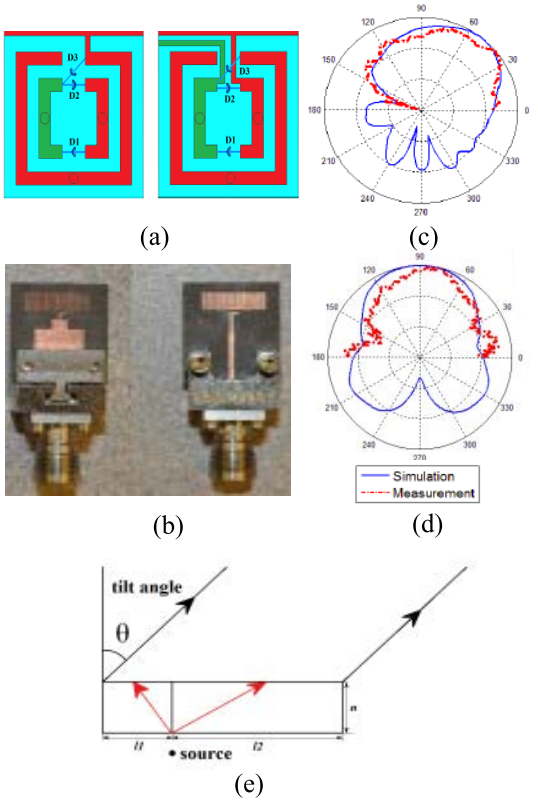

FIGURE 13. The dipole antenna of [145] with the reconfigurable SRR: (a) top and bottom views of the reconfigurable SRR, (b) the fabricated dipole antenna loaded by an array of SRRs, (c) and (d) the simulated and measured radiation patterns in E-plane and H-plane, respectively, (e) the beam deflection mechanism.

indices media in the way of electromagnetic rays emitting from the dipole antenna, which are displayed in Fig. 13(e) with lengths l_1 and l_2. The deflection angle can be predicted by the difference between the phase shift of the wave in two different media. The diagram in Fig. 13(e) shows the beam deflection mechanism. The average ray that enters the two configurations is given by

$$(l_a \times n_a) - (l_b \times n_b) = (l_a \times l_b) sin\,\theta \qquad (15)$$

where $l_a = \sqrt{(l_1/2 + n^2)}$ and $l_b = \sqrt{(l_2/2 + n^2)}$. For the proposed structure, $l_1 = 2.77$, $l_2 = 6.23$, and $n = 2.73$, the calculated deflection angle was 30°, which agreed with the simulated and measured results.

The reconfigurable MMs based on varactor diode were investigated in many studies, and used to control the antenna radiation pattern [147]–[150]. The main advantages of using a varactor diode are the multi-beam obtained by applying a varying bias voltage and using only one diode for unit cell reconfiguration, which helps to reduce the design and fabrication complexity. In [147], Errifi *et al.* used seven slabs, each with seven omega unit cells arranged vertically above the patch antenna for tilting the radiation pattern at 10 GHz [Fig. 14(a)]. Two varactor diodes were used to reconfigure each unit cell. By controlling the capacitance values of the two diodes, the positive angle of 30° and the negative

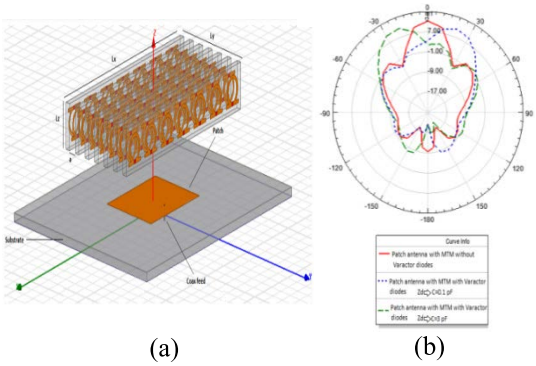

FIGURE 14. Patch antenna with omega shape unit cells based of [147]: (a) the schematic view of the MM antenna and (b) the radiation patterns of the MM antenna in the broadside direction at different capacitive; C = 0.1 pf (positive deflection) and C = 3 pf (negative deflection).

angle of −30° were obtained at capacitances of 0.1 pF and 3 pF, respectively. This is illustrated in Fig. 14(b). The beam tilting is due to the electromagnetic wave undergoing a phase change when passing through the air and MMs. Xie *et al.* [148] proposed reconfigurable composite right/left-handed transmission line (CRLH TL) unit cell based on varactor diode to manipulate the radiation pattern of the leaky-wave antenna (LWA). Varactor diodes were loaded into the unit cells for controlling the phase constant, thereby steering the radiation angle of the antenna from −66° to 62° in the broadside direction at 3 GHz. Sun *et al.* [149] proposed a reconfigurable I-shaped resonator based on varactor diodes to exhibit different refractive indices, which help to guide the antenna radiation beam to the desired direction. The incident wave transmits through the reconfigurable six MM layers and experiences different phase shifts after penetrating each layer. By applying low DC bias voltages to control the diodes of the MM layers, continuous scanning capability in a range of ±30° at the L-band was attained. The radiation pattern of the horn antenna was controlled by the s-ring structure loaded by varactor diodes [150]. The varactor diodes were used to change the phase of upcoming waves from the horn antenna, thereby steering it in the range of ±40° at 0.9 GHz. Luo *et al.* [151] used the MM based on MEMS switches to control the LWA radiation pattern. This report loads LWA by reconfigurable periodic J-shape unit cells to achieve deflection angles of ±15° at 8 GHz. Later, the same research group proposed tunable MM-based graphene, in which the unit cell consists of a metallic structure embedded by graphene [152]. The tunable MM-based graphene can be classified in two categories: (a) graphene-only plasmonic structures, and (b) graphene/metal hybrid MM structures. In the first type, the graphene is utilized as both the plasmonic media and the reconfigurable media, while in the second type graphene is used only as the reconfigurable media. The second type was used in this report, where the MM unit cell's surface conductivity was tuned by adjusting the chemical potential for producing different refractive indices, which helped to tilt the radiation pattern of the microstrip

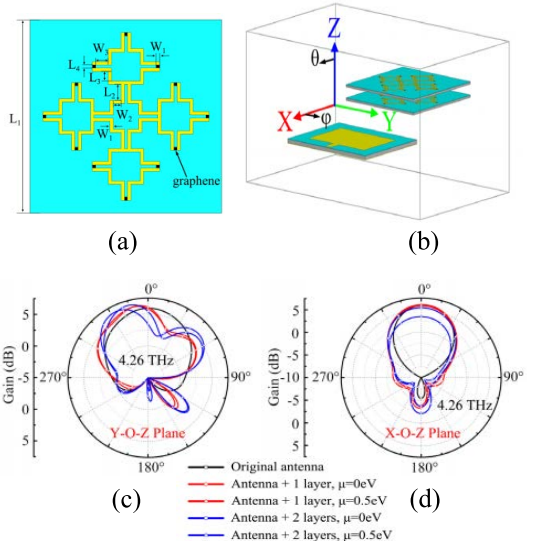

FIGURE 15. The microstrip antenna of [152] with two layers of tunable MMs: (a) the proposed unit cell-based graphene (b) the configuration of MM antenna, (c) and (d) the radiation patterns in the broadside direction (yoz-plane) and in xoz-plane.

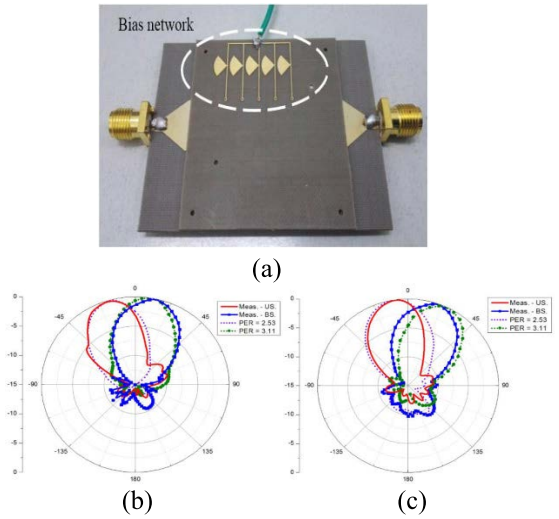

FIGURE 16. The reconfigurable MM antenna based of [153]: (a) the fabricated prototype, and the simulated and measured radiation patterns at (b) 7.2 GHz and (c) 9.4 GHz.

antenna at the terahertz regime. The beam deflection mechanism was explained based on the Snell's law as in [122]. The MM unit cell and microstrip antenna configurations with two layers of MMs are presented in Figs. 15(a) and (b), respectively. Using one layer of MMs and the chemical potential of 0.5 eV, the deflection angle of $-11°$ was obtained in the broadside direction (yoz-plane) with a gain enhancement of 0.43 dB. In contrast, the deflection angle was increased to $-27°$ with a gain improvement of 0.61 dB when using two layers and chemical potential of 0.5 eV at 4.26 THz. Figures 15(c) and (d) display the radiation patterns in the yoz-plane and xoz-plane, respectively, with different layers and chemical potentials.

The dual-band beam-steering antenna using tunable MM was proposed in [153]. The liquid crystal (LC) extended composite right/left-handed (E-CRLH) MM was arranged in layers to achieve the dual-band beam steering using tunable LC and an external voltage. The photograph of the MM antenna is shown in Fig. 16(a). By applying a bias voltage, the permittivity (PER) varies from 2.53 to 3.11 resulting in beam steering from $-16°$ to $13°$ at 7.2 GHz and $-9°$ to $17°$ at 9.4 GHz. The simulated and measured radiation patterns at 7.2 GHz and 9.4 GHz are presented in Figs. 16(b) and (c). Table 2 summarises the usage of reconfigurable MM for antenna beam deflection.

C. CONTROLLING THE ANTENNA RADIATED BEAM USING GRIN

As mentioned earlier, GRINs are realized by a slight variation in each consecutive component's properties along a direction perpendicular to the direction of propagation. The idea of utilizing GRIN to manipulate the propagation of electromagnetic waves was introduced by Smith *et al.* in [102], where the SRR was used to tilt the microwave beam. The spherical waves can be converted into planar ones with a deflection angle using the GRINs lens, as illustrated in Fig. 17. The radiation beam can be deflected by θ when the refractive index distribution of the MMs lens follows spatial position function, as follows [102], [154], [155]:

$$n = n_o - (y sin\theta + \sqrt{a^2 + y^2} - a)/t \tag{16}$$

where a denotes the distance between the electromagnetic wave source and the GRINs lens, n_0 is the refractive index at the centre location, $y = 0$ and $z = 0$. Here, y is the direction of refractive index distribution, and t is the thickness of the GRINs lens. Several studies were carried out to implement beam deflection antennas based on GRINs lens [154]–[159]. The beam deflection antenna based on the GRINs lens was demonstrated theoretically and experimentally by Liu *et al.* [154]. H-shape and square split-ring resonator were combined to form a unit cell. The MM unit cells were arranged vertically in 17 rows at the aperture of a horn antenna, cf. Fig. 18(a). The unit cells differ in size to exhibit a different refractive index of each row. The electromagnetic wave passes through the MM array and deflects by an angle of 10° at 15 GHz, as depicted in Fig. 18(b). This is, however, accompanied by the increased complexity and the overall size of the antenna system. In addition, the gain dropped by 0.48 dB. Ma *et al.* [155] proposed GRINs lens-based interdigital capacitor structure to deflect the radiation beam of the horn antenna by angles of 15° and 30° at 8 GHz. The lens antenna and the GRINs lens are shown in Fig. 19(a), whereas the measured electric field distributions that show the two deflection angles are depicted in Figs. 19(b) and (c). Furthermore, the six beam lens antenna was proposed by Aghanejad *et al.* [156], in which the antenna's main beam was converted into six beams using a non-resonant MM lens.

TABLE 2. Summary of beam deflection antennas using reconfigurable MMs.

Ref.	Antenna type	Frequency band	Beam deflection angle	Gain enhancement	Efficiency and (bandwidth)	Reconfigurable method	MM structure
[140]	Dipole antenna	Ka-band (28 GHz)	30° and −27° (E-plane)	Increased by 1.9 dB and 1.5 dB, respectively	90% (—)	Copper strip representing the real PIN diode	CSR
[141]	Dipole antenna	Ka-band (28 GHz)	34° and −30° (E-plane)	Increased by 1.7 dB and 1.5 dB, respectively	91% (Not affected)	Copper strip representing the real PIN diode	Bridge shape resonator (BSR)
[142]	Monopole antenna	L-band (1.17GHz)	90° and 270°	—	80% and 70%, respectively (—)	Copper strip representing the real PIN diode	capacitively loaded loop (CLL) rings
[143]	Monopole antenna	L-band (1.76 GHz)	▪ Tow SSR (90° and 270°) ▪ Three SRRs (45°,150°, and 270°) -Four SSRs (0°, 90°,180°, and 270°)	—	— (—)	Copper strip representing the real PIN diode	SRR
[145]	Dipole antenna	V band (60 GHz)	32°	Increased by 2.4 dB	— (Not affected)	PIN diode	SRR
[147]	Patch antenna	X-band (10 GHz)	±30°	Increased by 2.58 dB	— (Increased by 5%)	Varactor diode	Omega shape
[148]	Leaky-wave antenna	S-band (3.0 GHz)	Scanning angle form −66° to 62°	—	Over 50% (—)	Varactor diode	CRLH TL
[149]	MM antenna	L-band (1.42-1.63 GHz)	±30°	Decreased by 3 dB	— (—)	Varactor diode	I-shaped resonator
[150]	Horn antenna	L-band (0.9 GHz)	±40° scanning range	—	— (—)	Varactor diode	S-ring structure
[151]	Leaky-wave antenna	X band (8 GHz)	±15°	—	— (—)	MEMS	J-shape
[152]	Microstrip antenna	Terahertz (4.26 THz)	▪ One unit cell (−11°) ▪ Two unit cells (−27°)	-One unit cell (Increased by 0.43 dB) -Two unit cells (Increased by 0.61 dB	— (—)	Applying different chemical potentials	Metallic structure embedded graphene
[153]	Patch antenna	C-band (7.2 GHz) and X-band (9.4 GHz)	−16° to 13° at 7.2 GHz and − 9° to 17° at 9.4 GHz.	—	— (—)	Tunable LC by an external voltage	E-CRLH

The six beams of 5.09°, 60°, 117.2°, 171.3°, −109.9°, and −60° were obtained at 18 GHz by lens displacement. The mechanism of beam deflection is based on transformation optics. Xu *et al.* [157] proposed several 3D GRIN lenses to enhance the radiation characteristics of monopole antenna. These lenses were installed circularly around the monopole, which offered four beams and 10 dB of gain enhancement over 3-8 GHz. Nine layers of different permittivity values were presented by Jia *et al.* to form a GRIN lens [158]. These values were obtained by drilling holes with varying diameters in each layer. The beam steering was realized by rotating the feed horn along the focal plane. The maximum beam steering of 40° was obtained in the broadside direction at 12.5 and 14.25 GHz. Although the high steering angle was accomplished, the gain dropped by 2.5 dB. Dadgarpour *et al.* [159] discussed the implementation of beam deflection of the dipole antenna using GRINs based on a modified I-shaped resonator. The modified I-shaped resonator was presented in four forms to create variable refractive indices (tape A, B, C, and D). The report studied the beam deflection in three stages. In the first stage, the authors used one antenna with GRINs, in which the radiation pattern was deflected by 26° in E-plane with a gain improvement of 4 dB, as illustrated in Fig. 20(a). Two antennas were used in the second stage to achieve deflection angles of ±26°, as depicted in Fig. 20(b). In the last state, high deflection angles of ±56° were achieved using four antennas loaded by GRINs, as shown in Fig. 20(c). The beam deflection mechanism presented in [140] was applied here. The five rays of an electromagnetic wave travel over the four types of I-shaped in different lengths and directions, as shown in Fig. 20(d). The AF is given by

$$AF = 1 + e^{ikd_1 cos\gamma_1} + e^{ikd_2 cos\gamma_2} + \ldots + e^{ikd_5 cos\gamma_5} \quad (17)$$

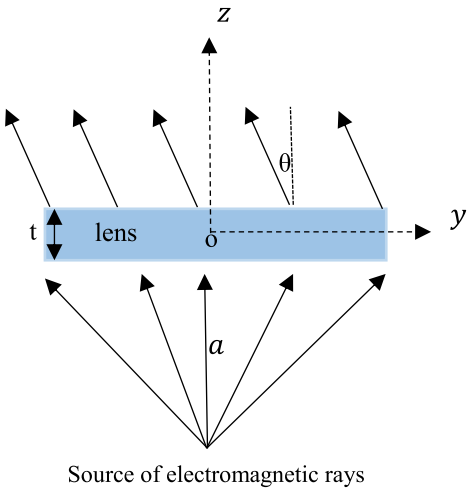

FIGURE 17. The basic operation of the GRINs as a lens.

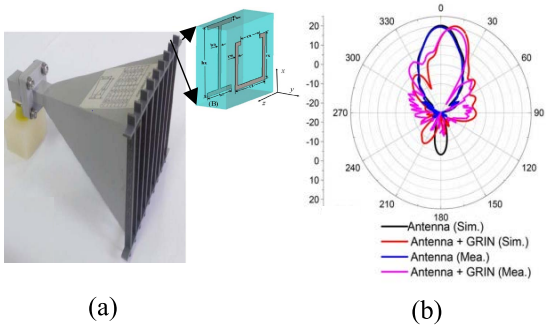

FIGURE 18. The horn antenna with GRIN lens based of [154]: (a) the fabricated array of GRIN; inset, the proposed MM structure, and (b) the simulated and measured radiation patterns at 15 GHz.

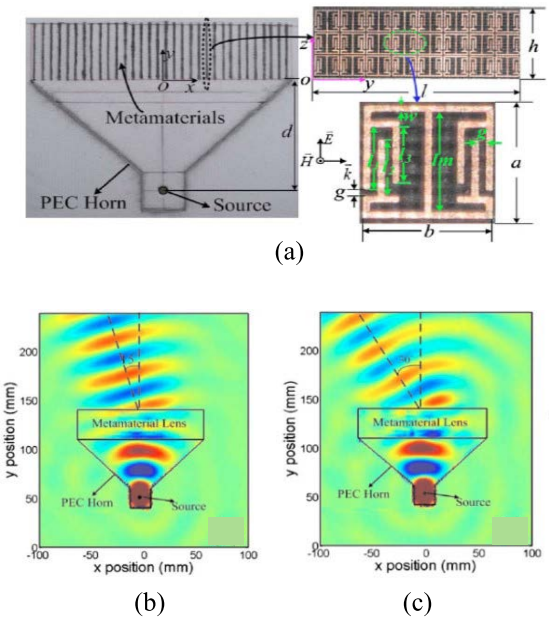

FIGURE 19. The horn antenna of [155] with GRIN lens: (a) the fabricated prototype, the measured electric field distributions at 8 GHz (b) 15° and (c) 30°.

The angles $\gamma_2, \ldots, \gamma_5$ were obtained by the dot product of the unit vector and the five vectors created by the rays. The far-field radiation pattern was calculated by multiplying the AF and the dipole antenna element factor. Table 3 gives the summary of the beam deflection based on GRINs.

The review carried out in this work leads to several observations concerning the design and realization of beam deflection antennas based on MMs. The following key aspects should be emphasized:

- Many techniques were introduced and employed to control the antenna radiation pattern, including electrical and mechanical approaches, and using the phased array antenna-based phase shifters, integrated lens antennas, the traveling wave antennas, and the beam-forming network (BFN) such as the Butler matrix. In phased array antennas, beam steering is made by means of phase shifters and attenuators associated with each one of the radiating elements that conforms to the antenna array. Designing the phase shifter with advanced electronic controls, achieving a wider scan-angle range, and reducing the feed network complexity and system physical size continue to be significant challenges for antenna designers. On the other hand, the beam-forming based on the Butler matrix comprises phase shifters, couplers, crossovers, and antennas, which are designed separately and then combined for a beam-forming purpose. The design complexity of each stage, large size, and narrow bandwidth are the main drawbacks of such a system. Furthermore, continuous steering is not possible as the radiation beam angle is connected to fixed input ports. In the integrated lens antennas and the traveling wave antennas methods, the large profile structure and unattainable multi-beam scenarios are the main shortcomings. It is expected that existing approaches, including the ones above, will be further improved by using MMs, especially in terms of alleviating the impairments of the traditional techniques. The design of MMs for controlling the antenna radiation pattern is considerably simple compared to the existing approaches, such as the Butler matrix and phased array antennas. The MMs with specific values of constitutive parameters, refractive index, permittivity, or permeability are arranged in the proximity of the radiating element for manipulating its beam. Further, the size of the MM antenna is more minor, whereas solely one antenna is integrated with small size unit cells ($< \lambda/4$). Moreover, the bandwidth is not limited, and the continued steering angle can be achieved using the reconfigurable MMs. Here, the advantages of the MMs over the traditional techniques can be summarized as follows:
  1. Simple feed network. A single feed antenna is used for obtaining the beam deflection system.
  2. The other antenna features, such as the gain and efficiency, can be enhanced / maintained by proper

TABLE 3. Summary of using GRINs for beam deflection antennas.

Ref.	Antenna type	Frequency band	Beam deflection angle	GRINs effect on the gain	Efficiency and (bandwidth)	Substrate material	MM structure
[154]	Horn antenna	Ku-band (15 GHz)	10°	Dropped by 0.48 dB	84.5% (__)	Teflon	SRR and H-shape
[155]	Horn antenna	X-band (8 GHz)	15° and 30°	__	__ (__)	F4B	Interdigital capacitor structure
[156]	Horn antenna	K-band (18 GHz)	5.09° , 60°, 117.2°, 171.3°, −109.9°, and −60°	__	__ (__)	__	Non-resonant MMs
[157]	Monopole antenna	C-band (5.5 GHz)	0°, 30°, 45° and 60°	Increased by 10 dB	>90% (Not affected)	F4B	Sierpinski fractal ring
[158]	Horn antenna	Ku-band (12.5 and 14.25 GHz)	40°	Dropped by 2.5 dB	74% at 12.5 65% at 14.25 GHz (__)	Dielectric laminate	Hole structure
[159]	Dipole antenna	V-band (57–64 GHz)	▪ One antenna 26° ▪ Two antennas ±26° ▪ Four antennas ±56°	Increased by 2.5 dB __ __	88.0% at 61 GHz (__)	Rogers RT5870	Modified I-shaped resonator

MMs design. Generally speaking, the antenna performance can be improved by including the MMs with appropriate constitutive parameters.

3. Small physical size system. Unlike the most common beam controlling approaches, Butler matrix and phased array antenna, only one antenna and an array of unit cells (size $< \lambda/4$) are integrated to manipulate the radiation pattern.
4. Less design complexity. After designing the antenna, the MM with particular values of constitutive parameters (refractive index, permittivity, or permeability) is only required for realizing the beam controlling system.
5. In contrast to the Butler matrix approach, the bandwidth is not limited, where it relies on the antenna design and even can be enhanced further by including the MMs.
6. Continued angle steering could be achieved by means of the reconfigurable MM based switches, but at the cost of increasing the complexity.

- Over the last two decades, considerable efforts have been devoted to realize beam deflection antennas by exploiting extraordinary characteristics of MMs, such as an array of MMs (with a positive/negative refractive index, ENZ, and MNZ), reconfigurable MMs, and GRIN MMs. In this respect, the degrees of freedom available to the designer when using these unique properties enable a wide range of beam tilting scenarios.
- The efficiency of beam deflection antenna based on MMs depends on the used approach. When including an array of MMs, the deflection angle is contingent upon the number of unit cells and their arrangement in front/above the radiating element. This approach yields a fixed deflection angle due to the stationary function of MMs. By using reconfigurable MMs, the type of switches and the complexity of their bias would affect the deflection angle. Besides, the inherent losses of some of these active devices degrade the system performance. Despite these impairments, this approach can achieve the multi-beam scenarios required by modern communication systems. The distribution of unit cells with a varying refractive index substantially affects the tilting angle when using the GRIN lens. The proper design can achieve a high deflection angle with maintaining/enhancing the gain performance.

VI. THE CHALLENGES AND FUTURE RESEARCH DIRECTIONS

In this section, some challenges in the designing of beam tilting antenna based MMs are presented as follows:

- The primary challenge in designing the MM antenna with beam tilting capability arises from the demanding specifications regarding performance expectations, e.g., gain, bandwidth, and efficiency. According to the presented literature, the reports focused on the gain performance, especially at the high-frequency range, where the high gain is instrumental for overcoming the path loss and providing a higher signal-to-noise ratio (SNR) at the receiver. Most works improved the gain performance by including MM array to antennas. However, others showed degradation in the gain for some reason. On the other hand, the bandwidth and efficiency have not been discussed in most presented reports, and only a few mention such features. Besides the beam tilting, enhancing/maintaining these features (gain, bandwidth, and efficiency) would require more investigation by

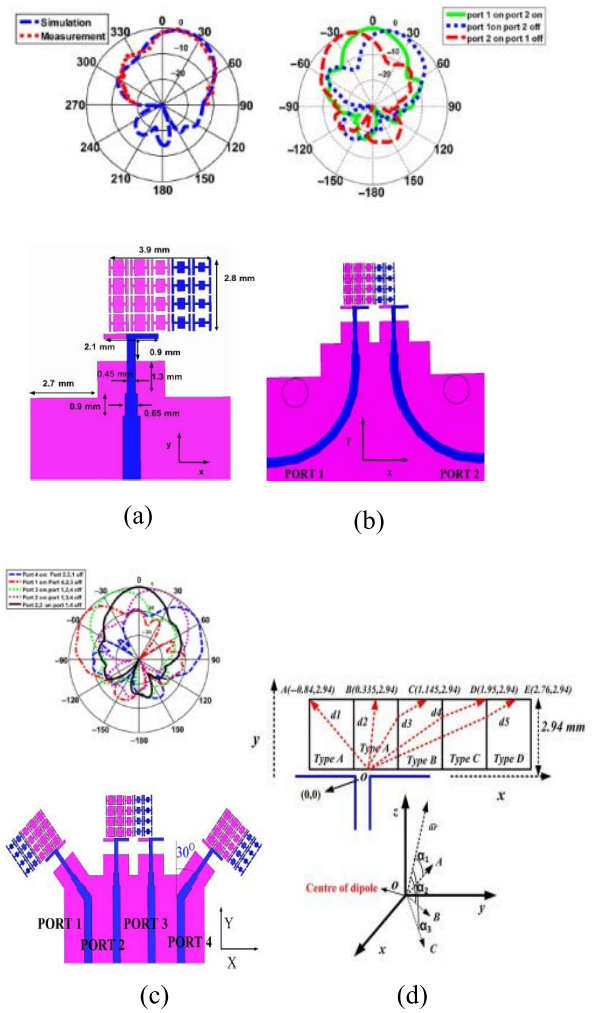

FIGURE 20. The dipole antenna with GRIN lens based of [159]: (a) using a single antenna, the deflection angle is 26° in E-plane, (b) using two antennas and changing the exciting ports, the deflection angles are ±26° in E-plane, (c) using four antennas, the deflection angles increased to ±56° in E-plane, and (d) beam deflection mechanism.

exploring different MM characteristics and integrating them with various antennas.

- Some characteristics of MMs are in demand for tilting the antenna radiation pattern, such as zero/near-zero refractive index, negative refractive index, ENZ, or MNZ, which are time-consuming to be achieved. Generally speaking, the MM design is based on geometry tailoring where there is no systematic method to attain such features. Here, formulating a solid theory behind MM characteristics that will accelerate the design process with desired performance is necessary.
- As presented in this survey, the reconfigurable MMs are the key to implementing the multi-beam antenna. However, achieving the reconfigurable MMs is challenging, especially at the high-frequency range, even with advanced micro/nanofabrication. This approach can provide a multi-beam antenna at the cost of design complexity. Moreover, the losses associated with some switches could cause degradation in antenna performance.

Some possible future research directions in the beam tilting antenna based MMs are summarized as follows:

- The millimeter-wave and terahertz spectrums have recently gained considerable attention due to their large bandwidth and high data rate, which are superior features for delivering the 5G and 6G technologies. The strong directionality and narrow beam of millimeter-wave and terahertz waves may easily cause the problem of local signal coverage holes and leads to signal transmission interruption. Thus, a functional device that realizes intelligent control of the antenna beam is urgently needed in millimeter-wave and terahertz communications, enabling flexible control of the beam's radiation direction and coverage area according to the actual communication requirement. Few reports implemented the beam deflection antenna-based MMs at both spectra. However, most of them controlled the antenna beam in one or two directions. The multi-beam antenna is instrumental in achieving the requirements mentioned above for the current 5G (millimeter-wave) and future 6G (terahertz), which reconfigurable MMs can achieve.
- The reconfigurable MMs-based electrical active switches (PIN and varactor diodes) were implemented in several reports to manipulate electromagnetic waves. Although these switches provide a multi-beam antenna, their high loss could affect other antenna features. The MEMS switches offer many benefits over alternative solutions, such as switching capability with high efficiency and isolation and moderate losses. However, only a few reports used such an approach for beam deflection application based on the presented works. This approach would require more exploration by integrating reconfigurable MM shapes based on MEMS with various antennas to increase the performance further.
- The tunable MM-based graphene is another promising approach, which can avoid the drawbacks of electrical switches. Multiple device structures have been proposed in the literature for realizing tunable MM-based graphene either by graphene-only plasmonic structures or graphene/metal hybrid MM structures. One of the main advantages of graphene resides in the possibility of integration into arbitrary substrates, i.e. low-loss. To the best of our knowledge, a handful of reports used this technique at the high-frequency range. This approach is of interest for realizing a multi-beam antenna without degradation in the other antenna features.
- The losses are crucial and need to be addressed during the design stage to avoid MM antenna performance degradation, especially at the high-frequency range. Using high conductivity metals such as silver or gold could help reduce the loss; however, ohmic loss of such metals is not avoidable. Recently, dielectric materials have been proposed to design low-loss antennas at a high-frequency range. Also, the dielectric MMs are studied as low-loss media. Therefore, combining both can

offer a low-loss beam deflection system. On the other hand, tunable MM-based graphene/MEMS can also provide a low-loss system

VII. CONCLUSION

This review paper provided an introduction to the MMs and discussed their electromagnetic behavior in the light of available literature. Moreover, their classification and design approaches were investigated, and reconfigurable MMs and their applications were introduced. In more depth, this review focused on the capability of MMs to manipulate the radiation characteristics of a broad range of antennas at different frequency spectra. Different MM properties such as the positive/negative refractive index, ENZ, and MNZ were exploited to realize the beam deflection by including their array form in the proximity of the radiating element, or into the same antenna substrate. This approach yielded a fixed deflection angle due to the stationary function of MMs. On the other hand, the reconfigurable MMs were loaded to antennas for beam deflection applications. Such an approach can be implemented by embedding active switches to the designed gaps of the MMs, which simultaneously deflects the radiation pattern in multiple directions, and reduces the overall size of the beam deflection system. Nevertheless, these switches increase the complexity of the antenna design and exhibit high losses. The GRIN lens is another beam deflection approach, which helps to focus the radiation beam from the antenna into the desired direction. The distribution of the refractive index, which follows the spatial position function, has a substantial effect on the performance of the beam deflection system.

APPENDIX

Nomenclature:

MMs	Metamaterials
ENZ	Epsilon-near-zero
MNZ	Mu near-zero
SRR	Split-ring resonator
GRIN	Gradient-Index
5G	Fifth generation
BFN	Beam-forming network
FSS	Frequency Selective Surface
AMC	Artificial Magnetic Conductor
EBG	Electromagnetic Band-Gap
RHMs	Right-handed materials
LHMs	Left-handed materials
DPS	Double-positive
ENG	Epsilon negative
MNG	Mu-negative
DNG	Double-negative materials
TL	Transmission line
NRIM	Negative refractive index material
MEMS	Micro-electro-mechanical systems
DGRs	Double G-shaped resonators
ELC	Electric-LC resonator
FL-LHM	Folded-line left-handed
DRA	Dielectric resonator antenna
DSR	Double split rectangular
SRRs	Square range resonators
ASSR	Adjacent square-shaped resonator
CLL	Capacitively loaded loop
CSRs	Contiguous squares resonator
AF	Array factor
CRLH TL	Composite right/left- handed transmission line
LWA	Leaky-wave antenna
LC	Liquid crystal
E-CRLH	Extended composite right/left-handed
BSR	Bridge shape resonator
SNR	Signal-to-noise ratio

REFERENCES

[1] M. Asif, D. A. Sehrai, S. H. Kiani, J. Khan, M. Abdullah, M. Ibrar, M. Alibakhshikenari, F. Falcone, and E. Limiti, "Design of a dual band SNG metamaterial based antenna for LTE 46/WLAN and Ka-band applications," *IEEE Access*, vol. 9, pp. 71553–71562, 2021.

[2] S. Zhang, W. Fan, N. C. Panoiu, K. J. Malloy, R. M. Osgood, and S. R. J. Brueck, "Experimental demonstration of near-infrared negative-index metamaterials," *Phys. Rev. Lett.*, vol. 95, no. 13, pp. 1–4, Sep. 2005.

[3] V. G. Veselago, "The electrodynamic of substances with simultaneous negative values of ϵ and μ," *Sov. Phys. Uspekhi*, vol. 10, no. 4, pp. 509–514, 1968.

[4] J. B. Pendry, A. J. Holden, W. J. Stewart, and I. Youngs, "Extremely low frequency plasmons in metallic mesostructures," *Phys. Rev. Lett.*, vol. 76, no. 25, pp. 4773–4776, 1996.

[5] J. B. Pendry, A. J. Holden, D. J. Robbins, and W. J. Stewart, "Magnetism from conductors and enhanced nonlinear phenomena," *IEEE Trans. Microw. Theory Techn.*, vol. 47, no. 11, pp. 2075–2084, Nov. 1999.

[6] D. R. Smith, W. J. Padilla, D. C. Vier, S. C. Nemat-Nasser, and S. Schultz, "Composite medium with simultaneously negative permeability and permittivity," *Phys. Rev. Lett.*, vol. 84, pp. 4184–4187, May 2000.

[7] S. Haxha, F. AbdelMalek, F. Ouerghi, M. D. B. Charlton, A. Aggoun, and X. Fang, "Metamaterial superlenses operating at visible wavelength for imaging applications," *Sci. Rep.*, vol. 8, no. 1, pp. 1–15, Dec. 2018.

[8] R. Dhama, B. Yan, C. Palego, and Z. Wang, "Super-resolution imaging by dielectric superlenses: TiO_2 metamaterial superlens versus $BaTiO_3$ superlens," *Photonics*, vol. 8, no. 6, pp. 1–9, 2021.

[9] A. Steckiewicz and A. Choroszucho, "Optimization-based synthesis of a metamaterial electric cloak using nonhomogeneous composite materials," *J. Electromagn. Waves Appl.*, vol. 33, no. 14, pp. 1933–1941, Sep. 2019.

[10] H. K. Zhang, Y. Chen, X. N. Liu, and G. K. Hu, "An asymmetric elastic metamaterial model for elastic wave cloaking," *J. Mech. Phys. Solids*, vol. 135, pp. 1–12, Feb. 2020.

[11] C. Tang, Q. Niu, Y. He, X. Zhang, and B. Wang, "Multiple-band terahertz metamaterial filter using coupling effect of U-type resonator and two same sizes of metallic split rings," *Mater. Res. Exp.*, vol. 6, no. 12, pp. 1–9, 2020.

[12] A. Khoshniat and R. Abhari, "Metamaterial absorbers for lining system shield box and packaging: Cavity analysis and equivalent material design," *IEEE Trans. Electromagn. Compat.*, vol. 63, no. 4, pp. 1007–1014, Aug. 2021.

[13] A. Bhardwaj, D. Pratap, K. Vaibhav Srivastava, and S. A. Ramakrishna, "Highly sensitive permittivity sensor using an inhomogeneous metamaterial cylindrical waveguide," *IEEE Sensors J.*, vol. 21, no. 7, pp. 9120–9127, Apr. 2021.

[14] J. Costantine, Y. Tawk, S. E. Barbin, and C. G. Christodoulou, "Reconfigurable antennas: Design and applications," *Proc. IEEE*, vol. 103, no. 3, pp. 424–437, Mar. 2015.

[15] Y. Zhou, R. S. Adve, and S. V. Hum, "Design and evaluation of pattern reconfigurable antennas for MIMO applications," *IEEE Trans. Antennas Propag.*, vol. 62, no. 3, pp. 1084–1092, Mar. 2014.

[16] N. O. Parchin, H. J. Basherlou, Y. I. A. Al-Yasir, A. M. Abdulkhaleq, and R. A. Abd-Alhameed, "Reconfigurable antennas: Switching techniques—A survey," *Electronics*, vol. 9, no. 2, pp. 12–14, 2020.

[17] E. Basar, M. Di Renzo, J. De Rosny, M. Debbah, M. Alouini, and R. Zhang, "Wireless communications through reconfigurable intelligent surfaces," *IEEE Access*, vol. 7, pp. 116753–116773, 2019.

[18] F. Zadehparizi and S. Jam, "Increasing reliability of frequency-reconfigurable antennas," *IEEE Antennas Wireless Propag. Lett.*, vol. 17, no. 5, pp. 920–923, May 2018.

[19] J. Zhu, B. Peng, and S. Li, "Cavity-backed high-gain switch beam antenna array for 60-GHz applications," *IET Micow. Antennas Propag.*, vol. 11, no. 12, pp. 1776–1781, Sep. 2017.

[20] D. K. Karmokar, K. P. Esselle, and S. G. Hay, "Fixed-frequency beam steering of microstrip leaky-wave antennas using binary switches," *IEEE Trans. Antennas Propag.*, vol. 64, no. 6, pp. 2146–2154, Jun. 2016.

[21] P. Liu, S. Yang, X. Wang, M. Yang, J. Song, and L. Dong, "Directivity-reconfigurable wideband two-arm spiral antenna," *IEEE Antennas Wireless Propag. Lett.*, vol. 16, pp. 66–69, 2017.

[22] J.-S. Row and Y.-H. Wei, "Wideband reconfigurable crossed-dipole antenna with quad-polarization diversity," *IEEE Trans. Antennas Propag.*, vol. 66, no. 4, pp. 2090–2094, Apr. 2018.

[23] B. A. F. Esmail, S. Koziel, and S. Szczepanski, "Overview of planar antenna loading metamaterials for gain performance enhancement: The two decades of progress," *IEEE Access*, vol. 10, pp. 27381–27403, 2022.

[24] H. W. Tian, W. Jiang, X. Li, Z. P. Chen, and T. J. Cui, "An ultrawideband and high-gain antenna based on 3-D impedance-matching metamaterial lens," *IEEE Trans. Antennas Propag.*, vol. 69, no. 6, pp. 3084–3093, Jun. 2021.

[25] D. Shan, H. Wang, K. Cao, and J. Zhang, "Wireless power transfer system with enhanced efficiency by using frequency reconfigurable metamaterial," *Sci. Rep.*, vol. 12, no. 1, pp. 1–11, Dec. 2022.

[26] M. Alibakhshikenari, B. S. Virdee, A. A. Althuwayb, L. Azpilicueta, N. O. Parchin, C. H. See, R. A. Abd-Alhameed, F. Falcone, I. Huynen, T. A. Denidni, and E. Limiti, "Bandwidth and gain enhancement of composite right left handed metamaterial transmission line planar antenna employing a non foster impedance matching circuit board," *Sci. Rep.*, vol. 11, no. 1, pp. 1–11, Dec. 2021.

[27] P. Dhanaraj and S. U. Maheswari, "Performance analysis of electrically coupled SRR bowtie antenna for wireless broadband communications," *Wireless Netw.*, vol. 26, no. 7, pp. 5271–5283, Oct. 2020.

[28] A. D. Tadesse, O. P. Acharya, and S. Sahu, "Application of metamaterials for performance enhancement of planar antennas: A review," *Int. J. RF Microw. Comput.-Aided Eng.*, vol. 30, no. 5, pp. 1–20, May 2020.

[29] A. I. Sulyman, A. T. Nassar, M. K. Samimi, G. R. Maccartney, T. S. Rappaport, and A. Alsanie, "Radio propagation path loss models for 5G cellular networks in the 28 GHZ and 38 GHZ millimeter-wave bands," *IEEE Commun. Mag.*, vol. 52, no. 9, pp. 78–86, Sep. 2014.

[30] H. Jiang, L.-M. Si, W. Hu, and X. Lv, "A symmetrical dual-beam bowtie antenna with gain enhancement using metamaterial for 5G MIMO applications," *IEEE Photon. J.*, vol. 11, no. 1, pp. 1–9, Feb. 2019.

[31] A. Dadgarpour, B. Zarghooni, B. S. Virdee, and T. A. Denidni, "Millimeter-wave high-gain SIW end-fire bow-tie antenna," *IEEE Trans. Antennas Propag.*, vol. 63, no. 5, pp. 2337–2342, May 2015.

[32] M. S. Khan, A. Iftikhar, A.-D. Capobianco, R. M. Shubair, and B. Ijaz, "Pattern and frequency reconfiguration of patch antenna using PIN diodes," *Microw. Opt. Technol. Lett.*, vol. 59, no. 9, pp. 2180–2185, Sep. 2017.

[33] S. Xiao, C. Zheng, M. Li, J. Xiong, and B.-Z. Wang, "Varactor-loaded pattern reconfigurable array for wide-angle scanning with low gain fluctuation," *IEEE Trans. Antennas Propag.*, vol. 63, no. 5, pp. 2364–2369, May 2015.

[34] I. F. da Costa, A. Cerqueira S., D. H. Spadoti, L. G. da Silva, J. A. J. Ribeiro, and S. E. Barbin, "Optically controlled reconfigurable antenna array for mm-wave applications," *IEEE Antennas Wireless Propag. Lett.*, vol. 16, pp. 2142–2145, 2017.

[35] Y. Zhang, S. Lin, S. Yu, G. J. Liu, and A. Denisov, "Design and analysis of optically controlled pattern reconfigurable planar Yagi–Uda antenna," *IET Microw., Antennas Propag.*, vol. 12, no. 13, pp. 2053–2059, Oct. 2018.

[36] A. Martin, V. Le Neillon, A. Jouade, and M. Himdi, "Mechanically reconfigurable radiation pattern slot antenna array feeded by bended sectoral horn and metalized wood splitter," *Prog. Electromagn. Res. C*, vol. 72, pp. 159–165, 2017.

[37] A. Mirkamali, R. Deban, F. Siaka, and J.-J. Laurin, "Fast and low-cost beam steering using an agile mechanical feed system for exciting circular arrays," *IET Microw., Antennas Propag.*, vol. 10, no. 4, pp. 378–384, Mar. 2016.

[38] J. Ala-Laurinaho, J. Aurinsalo, A. Karttunen, M. Kaunisto, A. Lamminen, J. Nurmiharju, A. V. Räisänen, J. Säily, and P. Wainio, "2-D beam-steerable integrated lens antenna system for 5G E-band access and backhaul," *IEEE Trans. Microw. Theory Techn.*, vol. 64, no. 7, pp. 2244–2255, Jul. 2016.

[39] S. K. Karki, J. Ala-Laurinaho, and V. Viikari, "Low-profile scanloss-reduced integrated metal-lens antenna," *IEEE Trans. Antennas Propag.*, vol. 70, no. 2, pp. 876–887, Feb. 2021.

[40] Y. Guo, Y. Guo, C. Li, H. Zhang, X. Zhou, and L. Zhang, "Integrated optical phased arrays for beam forming and steering," *Appl. Sci.*, vol. 11, no. 9, pp. 1–41, 2021.

[41] D. Dolfi, P. Joffre, J. Antoine, J.-P. Huignard, D. Philippet, and P. Granger, "Experimental demonstration of a phased-array antenna optically controlled with phase and time delays," *Appl. Opt.*, vol. 35, no. 26, pp. 5293–5300, Sep. 1996.

[42] T. Ueda, S. Yamamoto, Y. Kado, and T. Itoh, "Pseudo-traveling-wave resonator with magnetically tunable phase gradient of fields and its applications to beam-steering antennas," *IEEE Trans. Microw. Theory Techn.*, vol. 60, no. 10, pp. 3043–3054, Oct. 2012.

[43] R. Tchema, N. C. Papanicolaou, and A. C. Polycarpou, "An investigation of the dynamic beam-steering capability of a liquid-crystal-enabled leaky-wave antenna designed for 5G applications," *Appl. Phys. Lett.*, vol. 119, no. 3, pp. 1–6, 2021.

[44] B. T. Duyen, H. T. P. Thao, L. M. Thuy, and N. Q. Cuong, "Design of a beam steering antenna array using 8×8 butter matrix for indoor positioning system," *Electromagnetics*, vol. 40, no. 7, pp. 500–514, Oct. 2020.

[45] M. Jeon, Y. Seo, J. Cho, C. Lee, J. Jang, Y. Lee, H. W. Kwon, and S. Kahng, "Investigation on beam alignment of a microstrip-line Butler matrix and an SIW Butler matrix for 5G beamforming antennas through RF-to-RF wireless sensing and 64-QAM tests," *Sensors*, vol. 21, no. 20, pp. 1–27, 2021.

[46] J. R. Reis, R. F. S. Caldeirinha, A. Hammoudeh, and N. Copner, "Electronically reconfigurable FSS-inspired transmitarray for 2-D beamsteering," *IEEE Trans. Antennas Propag.*, vol. 65, no. 9, pp. 4880–4885, Sep. 2017.

[47] L. Han, G. Cheng, G. Han, R. Ma, and W. Zhang, "Electronically beam-steering antenna with active frequency-selective surface," *IEEE Antennas Wireless Propag. Lett.*, vol. 18, no. 1, pp. 108–112, Jan. 2019.

[48] W. Pan, C. Huang, P. Chen, M. Pu, X. Ma, and X. Luo, "A beam steering horn antenna using active frequency selective surface," *IEEE Trans. Antennas Propag.*, vol. 61, no. 12, pp. 6218–6223, Dec. 2013.

[49] G.-N. Zhou, B.-H. Sun, Q.-Y. Liang, Y.-H. Yang, and J.-H. Lan, "Beam-deflection short backfire antenna using phase-modulated metasurface," *IEEE Trans. Antennas Propag.*, vol. 68, no. 1, pp. 546–551, Jan. 2020.

[50] T. Hongnara, S. Chaimool, P. Akkaraekthalin, and Y. Zhao, "Design of compact beam-steering antennas using a Metasurface formed by uniform square rings," *IEEE Access*, vol. 6, pp. 9420–9429, 2018.

[51] T. Li and Z. N. Chen, "Control of beam direction for substrate-integrated waveguide slot array antenna using metasurface," *IEEE Trans. Antennas Propag.*, vol. 66, no. 6, pp. 2862–2869, Jun. 2018.

[52] Y. F. Cao and X. Y. Zhang, "A wideband beam-steerable slot antenna using artificial magnetic conductors with simple structure," *IEEE Trans. Antennas Propag.*, vol. 66, no. 4, pp. 1685–1694, Apr. 2018.

[53] F. Costa, A. Monorchio, S. Talarico, and F. M. Valeri, "An active high-impedance surface for low-profile tunable and steerable antennas," *IEEE Antennas Wireless Propag. Lett.*, vol. 7, pp. 676–680, 2009.

[54] A. R. Vilenskiy, V. I. Litun, and K. V. Lyulyukin, "Wideband beam steering antenna array of printed cavity-backed elements with integrated EBG structure," *IEEE Antennas Wireless Propag. Lett.*, vol. 18, no. 2, pp. 245–249, Feb. 2019.

[55] M. K. Abdulhameed, M. S. B. M. Isa, Z. Zakaria, I. M. Ibrahim, M. K. Mohsen, M. L. Attiah, and A. M. Dinar, "Radiation control of microstrip patch antenna by using electromagnetic band gap," *AEU-Int. J. Electron. Commun.*, vol. 110, Oct. 2019, Art. no. 152835.

[56] M. K. Abdulhameed, M. S. Mohamad Isa, Z. Zakaria, I. M. Ibrahim, and M. K. Mohsen, "Radiation pattern control of microstrip antenna in elevation and azimuth planes using EBG and pin diode," *Int. J. Electr. Comput. Eng.*, vol. 9, no. 1, pp. 332–340, 2019.

[57] B. A. F. Esmail, H. B. Majid, S. H. Dahlan, Z. Z. Abidin, M. K. A. Rahim, and M. Jusoh, "Planar antenna beam deflection using low-loss metamaterial for future 5G applications," *Int. J. RF Microw. Comput.-Aided Eng.*, vol. 29, no. 10, pp. 1–11, Oct. 2019.
[58] H. Barati, M. H. Fakheri, and A. Abdolali, "Experimental demonstration of metamaterial-assisted antenna beam deflection through folded transformation optics," *J. Opt.*, vol. 20, no. 8, pp. 1–16, 2018.
[59] N. O. Parchin, H. J. Basherlou, Y. Al-Yasir, R. Abd-Alhameed, A. Abdulkhaleq, and J. Noras, "Recent developments of reconfigurable antennas for current and future wireless communication systems," *Electronics*, vol. 8, no. 2, pp. 1–17, 2019.
[60] M. K. Shereen, M. I. Khattak, and G. Witjaksono, "A brief review of frequency, radiation pattern, polarization, and compound reconfigurable antennas for 5G applications," *J. Comput. Electron.*, vol. 18, no. 3, pp. 1065–1102, 2019.
[61] I. Uchendu and J. R. Kelly, "Survey of beam steering techniques available for millimeter wave applications," *Prog. Electromagn. Res. B*, vol. 68, pp. 35–54, 2016.
[62] X. Fu, F. Yang, C. Liu, X. Wu, and T. J. Cui, "Terahertz beam steering technologies: From phased arrays to field-programmable metasurfaces," *Adv. Opt. Mater.*, vol. 8, no. 3, pp. 1–22, 2020.
[63] M. K. Abdulhameed, M. M. Isa, I. M. Ibrahim, M. S. I. M. Zin, Z. Zakaria, M. K. Mohsin, and M. F. Alrifaie, "Review of radiation pattern control characteristics for the microstrip antenna based on electromagnetic band gap (EBG)," *J. Telecommun. Electron. Comput. Eng.*, vol. 10, no. 3, pp. 129–140, 2018.
[64] S. M. Kamali, E. Arbabi, A. Arbabi, and A. Faraon, "A review of dielectric optical metasurfaces for wavefront control," *Nanophotonics*, vol. 7, no. 6, pp. 1041–1068, 2018.
[65] J. D. Jackson, *Classical Electromagnetics*, 3rd ed. New York, NY, USA: Wiley, 1999.
[66] Y. Liu and X. Zhang, "Metamaterials: A new frontier of science and technology," *Chem. Soc. Rev.*, vol. 40, pp. 2494–2507, Dec. 2011, doi: 10.1039/c0cs00184h.
[67] C. Sabah and S. Uckun, "Multilayer system of Lorentz/Drude type metamaterials with dielectric slabs and its application to electromagnetic filters," *Prog. Electromagn. Res.*, vol. 91, pp. 349–364, 2009.
[68] J. T. Costa, M. G. Silveirinha, and A. Alù, "Poynting vector in negative-index metamaterials," *Phys. Rev. B, Condens. Matter*, vol. 83, no. 16, pp. 1–8, Apr. 2011.
[69] T. M. Grzegorczyk, C. D. Moss, J. Lu, X. Chen, J. Pacheco, and J. A. Kong, "Properties of left-handed metamaterials: Transmission, backward phase, negative refraction, and focusing," *IEEE Trans. Microw. Theory Techn.*, vol. 53, no. 9, pp. 2956–2966, Sep. 2005.
[70] S. H. Lee, C. M. Park, Y. M. Seo, and C. K. Kim, "Reversed Doppler effect in double negative metamaterials," *Phys. Rev. B, Condens. Matter*, vol. 81, no. 24, pp. 1–4, Jun. 2010.
[71] S. Xi, H. Chen, T. Jiang, L. Ran, J. Huangfu, B.-I. Wu, J. A. Kong, and M. Chen, "Experimental verification of reversed Cherenkov radiation in left-handed metamaterial," *Phys. Rev. Lett.*, vol. 103, no. 19, pp. 1–4, Nov. 2009.
[72] J. B. Pendry, A. J. Holden, D. J. Robbins, and W. J. Stewart, "Low frequency plasmons in thin-wire structures," *J. Phys. Condens. Matter*, vol. 10, no. 22, pp. 4785–4809, Jun. 1998.
[73] J. P. Turpin, J. A. Bossard, K. L. Morgan, D. H. Werner, and P. L. Werner, "Reconfigurable and tunable metamaterials: A review of the theory and applications," *Int. J. Antennas Propag.*, vol. 2014, pp. 1–18, May 2014.
[74] N. I. Zheludev and E. Plum, "Reconfigurable nanomechanical photonic metamaterials," *Nature Nanotechnol.*, vol. 11, no. 1, pp. 16–22, Jan. 2016.
[75] G. Zhang, H. Ma, C. Lan, R. Gao, and J. Zhou, "Microwave tunable metamaterial based on semiconductor-to-metal phase transition," *Sci. Rep.*, vol. 7, no. 1, pp. 1–6, Dec. 2017.
[76] L. Bao and T. J. Cui, "Tunable, reconfigurable, and programmable metamaterials," *Microw. Opt. Technol. Lett.*, vol. 62, no. 1, pp. 9–32, Jan. 2020.
[77] R. Dewan, M. K. A. Rahim, M. Himdi, M. R. Hamid, H. A. Majid, and M. E. Jalil, "Multiband frequency-reconfigurable antenna using metamaterial structure of electromagnetic band gap," *Appl. Phys. A, Solids Surf.*, vol. 123, no. 1, pp. 1–7, Jan. 2017.
[78] B. A. F. Esmail, H. A. Majid, Z. Z. Abidin, S. H. Dahlan, and M. K. A. Rahim, "Reconfigurable metamaterial structure at millimeter wave frequency range," *Int. J. Electr. Comput. Eng.*, vol. 7, no. 6, pp. 2942–2949, 2017.
[79] B. A. F. Esmail, H. A. Majid, Z. Z. Abidin, S. H. Dahlan, O. Ayop, and M. K. A. Rahim, "Refractive index reconfigurable metamaterial structure at 28 GHz frequency range," in *Proc. IEEE Asia Pacific Microw. Conf. (APMC)*, Nov. 2017, pp. 1325–1328.
[80] M. M. Hasan, E. Ahamed, M. R. I. Faruque, M. T. Islam, and S. Abdullah, "Reconfigurable metamaterial for 5G application," *J. Optoelectron. Adv. Mater.*, vol. 20, nos. 7–8, pp. 379–384, 2018.
[81] M. R. Hashemi, S. Cakmakyapan, and M. Jarrahi, "Reconfigurable metamaterials for terahertz wave manipulation," *Rep. Prog. Phys.*, vol. 80, no. 9, Sep. 2017, Art. no. 094501.
[82] F. Ma, Y. S. Lin, X. Zhang, and C. Lee, "Tunable multiband terahertz metamaterials using a reconfigurable electric split-ring resonator array," *Light Sci. Appl.*, vol. 3, no. e171, pp. 1–8, 2014.
[83] C. Yang, M. Boorugu, A. Dopp, J. Ren, R. Martin, D. Han, W. Choi, and H. Lee, "4D printing reconfigurable, deployable and mechanically tunable metamaterials," *Mater. Horizons*, vol. 6, no. 6, pp. 1244–1250, 2019.
[84] K. Fan and W. J. Padilla, "Dynamic electromagnetic metamaterials," *Materialstoday*, vol. 18, no. 1, pp. 39–50, Jan. /Feb. 2015.
[85] X. Duan, S. Chen, H. Cheng, Z. Li, and J. Tian, "Dynamically tunable plasmonically induced transparency by planar hybrid metamaterial," *Opt. Lett.*, vol. 38, no. 4, pp. 483–485, 2013.
[86] H. Yuan, B. O. Zhu, and Y. Feng, "A frequency and bandwidth tunable metamaterial absorber in x-band," *J. Appl. Phys.*, vol. 117, no. 17, pp. 1–6, 2015.
[87] J. Zhao, Q. Cheng, J. Chen, M. Q. Qi, W. X. Jiang, and T. J. Cui, "A tunable metamaterial absorber using varactor diodes," *New J. Phys.*, vol. 15, no. 4, pp. 1–11, 2013.
[88] B. Belkadi, Z. Mahdjoub, M. L. Seddiki, and M. Nedil, "A selective frequency reconfigurable bandstop metamaterial filter for WLAN applications," *Turkish J. Electr. Eng. Comput. Sci.*, vol. 26, no. 6, pp. 2976–2985, 2018.
[89] D. Lee, H. Jeong, and S. Lim, "Electronically switchable broadband metamaterial absorber," *Sci. Rep.*, vol. 7, no. 1, pp. 1–10, Dec. 2017.
[90] R. Amiri, B. Zarghooni, A. Dadgarpour, J. Pourahmadazar, and T. A. Denidni, "Reconfigurable metamaterial unit-cell with controllable refractive index," in *Proc. 17th Int. Symp. Antenna Technol. Appl. Electromagn. (ANTEM)*, Jul. 2016, pp. 1–2.
[91] I. G. Lee and I. P. Hong, "Design of a flexible and reconfigurable frequency selective surface," *Int. J. Circuits, Syst. Signal Process.*, vol. 9, pp. 296–299, Aug. 2015.
[92] D. Bouyge, A. Crunteanu, M. Durán-Sindreu, A. Pothier, P. Blondy, J. Bonache, J. C. Orlianges, and F. Martín, "Reconfigurable split rings based on MEMS switches and their application to tunable filters," *J. Opt.*, vol. 14, no. 11, pp. 1–9, 2012.
[93] C. P. Ho, P. Pitchappa, Y. S. Lin, C. Y. Huang, P. Kropelnicki, and C. Lee, "Electrothermally actuated microelectromechanical systems based omega-ring terahertz metamaterial with polarization dependent characteristics," *Appl. Phys. Lett.*, vol. 104, no. 16, pp. 1–5, 2014.
[94] S. Bang, J. Kim, G. Yoon, T. Tanaka, and J. Rho, "Recent advances in tunable and reconfigurable metamaterials," *Micromachines*, vol. 9, no. 11, pp. 1–23, 2018.
[95] K. Yang, S. Liu, S. Arezoomandan, A. Nahata, and B. Sensale-Rodriguez, "Graphene-based tunable metamaterial terahertz filters," *Appl. Phys. Lett.*, vol. 105, no. 9, pp. 1–4, 2014.
[96] H.-T. Chen, W. J. Padilla, J. M. O. Zide, A. C. Gossard, A. J. Taylor, and R. D. Averitt, "Active terahertz metamaterial devices," *Nature*, vol. 444, no. 7119, pp. 597–600, Nov. 2006.
[97] X. J. He, T. Y. Li, L. Wang, J. M. Wang, J. X. Jiang, G. H. Yang, F. Y. Meng, and Q. Wu, "Electrically tunable terahertz wave modulator based on complementary metamaterial and graphene," *J. Appl. Phys.*, vol. 115, no. 17, pp. 1–3, 2014.
[98] B. Zarghooni and T. A. Denidni, "New fractal metamaterial unit-cell for microwave applications," in *Proc. 8th Eur. Conf. Antennas Propag. (EuCAP)*, Apr. 2014, pp. 978–979.
[99] B. A. F. Esmail, M. K. A. Rahim, H. A. Majid, N. A. Murad, N. A. Samsuri, O. Ayop, A. Salh, and N. Al-Fadhali, "Deflected beam pattern through reconfigurable metamaterial structure at 3.5 GHz for 5G applications," *Waves Random Complex Media*, pp. 1–24, Mar. 2022, doi: 10.1080/17455030.2022.2053608.
[100] Y. Zheng, J. Gao, Y. Zhou, X. Cao, H. Yang, S. Li, and T. Li, "Wideband gain enhancement and RCS reduction of Fabry–Perot resonator antenna with chessboard arranged metamaterial superstrate," *IEEE Trans. Antennas Propag.*, vol. 66, no. 2, pp. 590–599, Feb. 2018.

[101] R. Liu, X. M. Yang, J. G. Gollub, J. J. Mock, T. J. Cui, and D. R. Smith, "Gradient index circuit by waveguided metamaterials," *Appl. Phys. Lett.*, vol. 94, no. 7, pp. 1–3, 2009.

[102] D. R. Smith, J. J. Mock, A. F. Starr, and D. Schurig, "Gradient index metamaterials," *Phys. Rev. E, Stat. Phys. Plasmas Fluids Relat. Interdiscip. Top.*, vol. 71, no. 3, pp. 1–6, Mar. 2005.

[103] R. B. Greegor, C. G. Parazzoli, J. A. Nielsen, M. A. Thompson, M. H. Tanielian, and D. R. Smith, "Simulation and testing of a graded negative index of refraction lens," *Appl. Phys. Lett.*, vol. 87, no. 9, pp. 1–4, 2005.

[104] T. Driscoll, D. N. Basov, P. M. Rye, S. Nemat-Nasser, D. Schurig, and D. R. Smith, "Free space microwave focusing by a negative-index gradient lens," *Complex Photonic Media*, vol. 6320, no. 1, pp. 1–3, 2006.

[105] H. Ma, X. Chen, X. Yang, H. Xu, Q. Cheng, and T. Cui, "A broadband metamaterial cylindrical lens antenna," *Chin. Sci. Bull.*, vol. 55, no. 19, pp. 2066–2070, 2010.

[106] Q. Cheng, H. F. Ma, and T. J. Cui, "Broadband planar Luneburg lens based on complementary metamaterials," *Appl. Phys. Lett.*, vol. 95, no. 18, pp. 2012–2015, 2009.

[107] L. Yin, J. Doyhamboure–Fouquet, X. Tian, and D. Li, "Design and characterization of radar absorbing structure based on gradient-refractive-index metamaterials," *Composites B, Eng.*, vol. 132, pp. 178–187, Jan. 2018.

[108] B. Ganapathy and S. C. Krishnaswamy, "Energy transfer using gradient index metamaterial," *Int. J. Antennas Propag.*, vol. 2018, pp. 1–6, Jan. 2018.

[109] B. P. Mishra, S. Sahu, S. K. S. Parashar, and S. K. Pathak, "A compact wideband and high gain GRIN metamaterial lens antenna system suitable for C, X, Ku band application," *Optik*, vol. 165, pp. 266–274, Jul. 2018.

[110] X. Chen, H. Ma, X. Yang, Q. Cheng, W. X. Jiang, and T. J. Cui, "X-band high directivity lens antenna realized by gradient index metamaterials," in *Proc. Asia Pacific Microw. Conf.*, Dec. 2009, pp. 793–797.

[111] R. Singha and D. Vakula, "Low side lobe tapered slot antenna with high gain using gradient refractive index metamaterial for ultra wideband application," *Adv. Electromagn.*, vol. 6, no. 4, pp. 63–69, Nov. 2017.

[112] H. F. Ma, G. Z. Wang, W. X. Jiang, and T. J. Cui, "Independent control of differently-polarized waves using anisotropic gradient-index metamaterials," *Sci. Rep.*, vol. 4, no. 1, pp. 1–8, May 2015.

[113] X. Q. Lin, T. J. Cui, J. Y. Chin, X. M. Yang, Q. Cheng, and R. Liu, "Controlling electromagnetic waves using tunable gradient dielectric metamaterial lens," *Appl. Phys. Lett.*, vol. 92, no. 13, pp. 1–3, 2008.

[114] W. X. Jiang, H. F. Ma, and T. J. Cui, "Planar reflector antenna design based on gradient-index metamaterials," in *Proc. Int. Conf. Microw. Millim. Wave Technol.*, May 2010, pp. 431–433.

[115] A. Dadgarpour, B. Zarghooni, B. S. Virdee, and T. A. Denidni, "Beam tilting antenna using integrated metamaterial loading," *IEEE Trans. Antennas Propag.*, vol. 62, no. 5, pp. 2874–2879, May 2014.

[116] A. Dadgarpour, B. Zarghooni, B. S. Virdee, and T. A. Denidni, "Enhancement of tilted beam in elevation plane for planar end-fire antennas using artificial dielectric medium," *IEEE Trans. Antennas Propag.*, vol. 63, no. 10, pp. 4540–4545, Oct. 2015.

[117] A. Ourir, S. N. Burokur, and A. De Lustrac, "Phase-varying metamaterial for compact steerable directive antennas," *Electron. Lett.*, vol. 43, no. 9, pp. 40–41, 2007.

[118] A. Ghasemi, S. N. Burokur, A. Dhouibi, and A. de Lustrac, "Inductive-varying grid for highly beamsteerable cavity antennas," *Electron. Lett.*, vol. 49, no. 5, pp. 319–321, Feb. 2013.

[119] J. Yi, A. de Lustrac, and S. N. Burokur, "Metamaterial lens for beam steering," in *Proc. 10th Eur. Conf. Antennas Propag. (EuCAP)*, Apr. 2016, pp. 9–12.

[120] M. T. Le, Q. C. Nguyen, and T. P. Vuong, "Design of high-gain and beam steering antennas using a new planar folded-line metamaterial structure," *Int. J. Antennas Propag.*, vol. 2014, pp. 1–16, Jan. 2014.

[121] Y. Li, M. F. Iskander, Z. Zhang, and Z. Feng, "A new low cost leaky wave coplanar waveguide continuous transverse stub antenna array using metamaterial-based phase shifters for beam steering," *IEEE Trans. Antennas Propag.*, vol. 61, no. 7, pp. 3511–3518, Jul. 2013.

[122] J. Li, Q. Zeng, R. Liu, and T. A. Denidni, "Beam-tilting antenna with negative refractive index metamaterial loading," *IEEE Antennas Wireless Propag. Lett.*, vol. 16, pp. 2030–2033, 2017.

[123] A. Dadgarpour, B. Zarghooni, T. A. Denidni, and A. A. Kishk, "Dual-band radiation tilting endfire antenna for WLAN applications," *IEEE Antennas Wireless Propag. Lett.*, vol. 15, pp. 1466–1469, 2016.

[124] A. Dadgarpour, A. A. Kishk, and T. A. Denidni, "Dual band high-gain antenna with beam switching capability," *IET Microw., Antennas Propag.*, vol. 11, no. 15, pp. 2155–2161, Oct. 2017.

[125] V. Pacheco-Peña, V. Torres, B. Orazbayev, M. Beruete, M. Navarro-Cia, M. Sorolla, and N. Engheta, "Mechanical 144 GHz beam steering with all-metallic epsilon-near-zero lens antenna," *Appl. Phys. Lett.*, vol. 105, no. 24, pp. 1–5, 2014.

[126] A. Dadgarpour, B. Zarghooni, and T. A. Denidni, "Beamforming bow-tie antenna for millimeter-wave applications using metamaterial lens," in *Proc. IEEE Int. Symp. Antennas Propag. USNC/URSI Nat. Radio Sci. Meeting*, Jul. 2015, pp. 254–255.

[127] A. Dadgarpour, B. Zarghooni, B. S. Virdee, and T. A. Denidni, "Improvement of gain and elevation tilt angle using metamaterial loading for millimeter-wave applications," *IEEE Antennas Wireless Propag. Lett.*, vol. 15, pp. 418–420, 2016.

[128] B. A. F. Esmail, H. A. Majid, S. H. Dahlan, Z. Z. Abidin, M. K. A. Rahim, M. A. Abdullah, and M. Jusoh, "Antenna beam tilting and gain enhancement using novel metamaterial structure at 28 GHz," in *Proc. IEEE Int. RF Microw. Conf. (RFM)*, Penang, Malaysia, Dec. 2018, pp. 53–56.

[129] A. Dadgarpour, B. Zarghooni, B. S. Virdee, and T. A. Denidni, "One- and two-dimensional beam-switching antenna for millimeter-wave MIMO applications," *IEEE Trans. Antennas Propag.*, vol. 64, no. 2, pp. 564–573, Feb. 2016.

[130] A. Dadgarpour, M. S. Sorkherizi, T. A. Denidni, and A. A. Kishk, "Passive beam switching and dual-beam radiation slot antenna loaded with ENZ medium and excited through ridge gap waveguide at millimeter-waves," *IEEE Trans. Antennas Propag.*, vol. 65, no. 1, pp. 92–102, Jan. 2017.

[131] J. B. Pendry, D. Schurig, and D. R. Smith, "Controlling electromagnetic fields," *Science*, vol. 312, no. 5781, pp. 1780–1782, May 2006.

[132] X. Jing, D. Feng, Y. Tian, M. Li, C. Chu, C. Li, Y. He, H. Gan, and Z. Hong, "Design of two invisibility cloaks using transmissive and reflective metamaterial-based multilayer frame microstructures," *Opt. Exp.*, vol. 28, no. 24, pp. 35528–35539, 2020.

[133] H. Chen and C. T. Chan, "Transformation media that rotate electromagnetic fields," *Appl. Phys. Lett.*, vol. 90, no. 24, pp. 2011–2014, 2007.

[134] L. Liang and S. V. Hum, "Realizing a flat UWB 2-D reflector designed using transformation optics," *IEEE Trans. Antennas Propag.*, vol. 62, no. 5, pp. 2481–2487, May 2014.

[135] Y. Lai, H. Chen, Z.-Q. Zhang, and C. T. Chan, "Complementary media invisibility cloak that cloaks objects at a distance outside the cloaking shell," *Phys. Rev. Lett.*, vol. 102, no. 9, pp. 1–4, Mar. 2009.

[136] C. Yang, M. Huang, J. Yang, F. Mao, and P. Li, "Design of open devices based on multi-folded transformation optics," *J. Phys. Commun.*, vol. 4, no. 4, pp. 1–11, 2020.

[137] H. A. Madni, K. Hussain, W. X. Jiang, S. Liu, A. Aziz, S. Iqbal, A. Mahboob, and T. J. Cui, "A novel EM concentrator with open-concentrator region based on multi-folded transformation optics," *Sci. Rep.*, vol. 8, no. 1, pp. 1–10, Dec. 2018.

[138] Q. L. Zhang, B. J. Chen, K. F. Chan, and C. H. Chan, "High-gain millimeter-wave antennas based on spoof surface plasmon polaritons," *IEEE Trans. Antennas Propag.*, vol. 68, no. 6, pp. 4320–4331, Jun. 2020.

[139] D. Chizhik, J. Du, R. Feick, M. Rodriguez, G. Castro, and R. A. Valenzuela, "Path loss and directional gain measurements at 28 GHz for non-line-of-sight coverage of indoors with corridors," *IEEE Trans. Antennas Propag.*, vol. 68, no. 6, pp. 4820–4830, Jun. 2020.

[140] B. A. Esmail, H. A. Majid, Z. Z. Abidin, S. H. Dahlan, M. Himdi, R. Dewan, M. K. A. Rahim, and N. Al-Fadhali, "Reconfigurable radiation pattern of planar antenna using metamaterial for 5G applications," *Materials*, vol. 13, no. 3, pp. 1–15, 2020.

[141] B. A. F. Esmail, H. A. Majid, S. H. Dahlan, Z. Z. Abidin, M. Himdi, R. Dewan, M. K. A. Rahim, and A. Y. I. Ashyap, "Reconfigurable metamaterial structure for 5G beam tilting antenna applications," *Waves Random Complex Media*, vol. 31, no. 6, pp. 2089–2102, Nov. 2021.

[142] S. Dakhli, H. Rmili, J.-M. Floc'h, M. Sheikh, K. Mahdjoubi, F. Choubani, and R. W. Ziolkowski, "Capacitively loaded loop-based antennas with reconfigurable radiation patterns," *Int. J. Antennas Propag.*, vol. 2015, pp. 1–10, Jun. 2015.

[143] S. Dakhli, J.-M. Floch, K. Mahdjoubi, H. Rmili, and F. Choubani, "A reconfigurable radiation pattern metamaterial-inspired circular array antenna," in *Proc. 8th Eur. Conf. Antennas Propag. (EuCAP)*, Apr. 2014, pp. 2566–2569.

[144] S. Yan and G. A. E. Vandenbosch, "Radiation pattern-reconfigurable wearable antenna based on metamaterial structure," *IEEE Antennas Wireless Propag. Lett.*, vol. 15, pp. 1715–1718, 2016.
[145] B. Zarghooni, A. Dadgarpour, and T. A. Denidni, "Millimeter-wave antenna using two-sectioned metamaterial medium," *IEEE Antennas Wireless Propag. Lett.*, vol. 15, pp. 960–963, 2016.
[146] M. R. Islam and M. Ali, "Elevation plane beam scanning of a novel parasitic array radiator antenna for 1900 MHz mobile handheld terminals," *IEEE Trans. Antennas Propag.*, vol. 58, no. 10, pp. 3344–3352, Oct. 2010.
[147] H. Errifi, A. Baghdad, A. Badri, and A. Sahel, "Directive beam-steering patch antenna using adjustable metamaterial superstrate," in *Proc. Int. Symp. Ubiquitous Netw.*, 2015, pp. 183–194.
[148] S. Xie, J. Li, G. Deng, J. Feng, and S. Xiao, "A wide-angle scanning leaky-wave antenna based on a composite right/left-handed transmission line," *Appl. Sci.*, vol. 10, no. 6, pp. 1–10, 2020.
[149] Y. Sun, Z. Li, W. Zhu, Z. Ji, and Q. Wang, "New steerable antenna with controllable metamaterial," in *Proc. 42nd Eur. Microw. Conf.*, Oct. 2012, pp. 936–939.
[150] H. Chen, B. I. Wu, L. Ran, T. M. Grzegorczyk, and J. A. Kong, "Controllable left-handed metamaterial and its application to a steerable antenna," *Appl. Phys. Lett.*, vol. 89, no. 5, pp. 136–139, 2006.
[151] Y. Luo, K. Kikuta, Z. Han, T. Takahashi, A. Hirose, and H. Toshiyoshi, "An active metamaterial antenna with MEMS-modulated scanning radiation beams," *IEEE Electron Device Lett.*, vol. 37, no. 7, pp. 920–923, Jul. 2016.
[152] Y. Luo, Q. Zeng, X. Yan, T. Jiang, R. Yang, J. Wang, Y. Wu, Q. Lu, and X. Zhang, "A graphene-based tunable negative refractive index metamaterial and its application in dynamic beam-tilting terahertz antenna," *Microw. Opt. Technol. Lett.*, vol. 61, no. 12, pp. 2766–2772, Dec. 2019.
[153] B. Che, F. Meng, Y. Lyu, and Q. Wu, "Reconfigurable dual-band metamaterial antenna based on liquid crystals," *J. Phys. D, Appl. Phys.*, vol. 51, no. 18, pp. 1–7, 2018.
[154] Y. Liu, C. Liu, X. Jin, B. Zhang, Y. Zhang, X. Zhu, B. Su, and X. Zhao, "Beam steering by using a gradient refractive index metamaterial planar lens and a gradient phase metasurface planar lens," *Microw. Opt. Technol. Lett.*, vol. 60, no. 2, pp. 330–337, Feb. 2018.
[155] H. F. Ma, X. Chen, H. S. Xu, X. M. Yang, W. X. Jiang, and T. J. Cui, "Experiments on high-performance beam-scanning antennas made of gradient-index metamaterials," *Appl. Phys. Lett.*, vol. 95, no. 9, pp. 93–96, 2009.
[156] I. Aghanejad, H. Abiri, and A. Yahaghi, "Design of high-gain lens antenna by gradient-index metamaterials using transformation optics," *IEEE Trans. Antennas Propag.*, vol. 60, no. 9, pp. 4074–4081, Sep. 2012.
[157] H.-X. Xu, G.-M. Wang, Z. Tao, and T. J. Cui, "High-directivity emissions with flexible beam numbers and beam directions using gradient-refractive-index fractal metamaterial," *Sci. Rep.*, vol. 4, no. 1, pp. 1–10, May 2015.
[158] D. Jia, Y. He, N. Ding, J. Zhou, B. Du, and W. Zhang, "Beam-steering flat lens antenna based on multilayer gradient index metamaterials," *IEEE Antennas Wireless Propag. Lett.*, vol. 17, no. 8, pp. 1510–1514, Aug. 2018.
[159] A. Dadgarpour, B. Zarghooni, B. S. Virdee, and T. A. Denidni, "Beam-deflection using gradient refractive-index media for 60-GHz end-fire antenna," *IEEE Trans. Antennas Propag.*, vol. 63, no. 8, pp. 3768–3774, Aug. 2015.

BASHAR A. F. ESMAIL (Member, IEEE) received the B.Eng. degree (Hons.) in electrical engineering (telecommunications) from Ibb University, Yemen, in 2008, and the M.Eng. and Ph.D. degrees in electrical engineering from Universiti Tun Hussein Onn Malaysia, Malaysia, in 2016 and 2021, respectively. In 2021, he joined the Faculty of Engineering, School of Electrical Engineering, University of Technology Malaysia, Johor, Malaysia, as a Postdoctoral Researcher. He is currently working as a Postdoctoral Researcher with the Engineering Optimization and Modeling Center (EOMC), Department of Electrical Engineering, Reykjavik University, Iceland. His research interests include design of metamaterial structures, millimeter wave antenna, MIMO, and reconfigurable antennas.

SLAWOMIR KOZIEL (Fellow, IEEE) received the M.Sc. and Ph.D. degrees in electronic engineering from the Gdańsk University of Technology, Poland, in 1995 and 2000, respectively, and the M.Sc. degree in theoretical physics and the M.Sc. and Ph.D. degrees in mathematics from the University of Gdańsk, Poland, in 2000, 2002, and 2003, respectively. He is currently a Professor with the Department of Engineering, Reykjavik University, Iceland. His research interests include CAD and modeling of microwave and antenna structures, simulation-driven design, surrogate-based optimization, space mapping, circuit theory, analog signal processing, evolutionary computation, and numerical analysis.

LUKASZ GOLUNSKI received the M.Sc. degree in materials engineering and the Ph.D. degree in electronic engineering from the Gdańsk University of Technology, Poland, in 2011 and 2018, respectively. He is currently an Assistant Professor with the Faculty of Electronics, Telecommunications and Informatics, Gdańsk University of Technology. His research interests include thin film growth, chemical vapor deposition and physical vapor methods, semiconductor diamond synthesis, and their electrical analysis.

HUDA BIN A. MAJID (Member, IEEE) received the Ph.D. degree in electrical engineering from Universiti Teknologi Malaysia (UTM). He worked as a Postdoctoral Fellow with UTM for a period of one year. He is currently a Lecturer with the Faculty Engineering Technology, Universiti Tun Hussein Onn Malaysia (UTHM), Batu Pahat, Johor. He has published over 100 articles in journals and conference papers. His research interests include planar and flexible antennas, array antennas, reconfigurable antennas, metamaterial, and RF microwave and mm-wave devices.

RUSAN KUMAR BARIK (Member, IEEE) received the B.Tech. degree in electronics and communication engineering from the Biju Patnaik University of Technology, Rourkela, India, in 2012, and the M.Tech. degree in communication systems design and the Ph.D. degree in electronics engineering from the Indian Institute of Information Technology, India, in 2015 and 2018, respectively. In 2018, he joined the Department of Electronics and Communication Engineering, Christ University, Bengaluru, India, as an Assistant Professor. In 2019, he joined the Department of Electrical and Electronic Engineering, Southern University of Science and Technology, Shenzhen, China, as a Postdoctoral Researcher. He is currently working as a Postdoctoral Researcher with the Engineering Optimization and Modeling Center (EOMC), Department of Electrical Engineering, Reykjavik University, Iceland. His research interests include multiband microwave devices, SIW components, surrogate-based modeling, and optimization.